



## **Influence of urban pollution on the production of organic particulate matter from isoprene epoxydiols in central Amazonia**

Suzane S. de Sá (1), Brett B. Palm (2), Pedro Campuzano-Jost (2), Douglas A. Day (2), Matthew K. Newburn (3), Weiwei Hu (2), Gabriel Isaacman-VanWertz<sup>a</sup> (4), Lindsay D. Yee (4), Ryan Thalman (5), Joel Brito<sup>b</sup> (6), Samara Carbone (6), Paulo Artaxo (6), Allen H. Goldstein (4), Antonio O. Manzi (7), Rodrigo A.F. Souza (8), Fan Mei (9), John E. Shilling (3,9), Stephen R. Springston (5), Jian Wang (5), Jason D. Surratt (10), M. Lizabeth Alexander (3), Jose L. Jimenez (2), Scot T. Martin<sup>\*</sup> (1, 11)

- (1) School of Engineering and Applied Sciences, Harvard University, Cambridge, Massachusetts, USA
- (2) Department of Chemistry & Biochemistry and Cooperative Institute for Research in Environmental Sciences, University of Colorado, Boulder, Colorado, USA
- (3) Environmental Molecular Sciences Laboratory, Pacific Northwest National Laboratory, Richland, Washington, USA
- (4) Dept. of Environmental Science, Policy, and Management, University of California, Berkeley, California, USA
- (5) Brookhaven National Laboratory, Upton, New York, USA
- (6) Departamento de Física Aplicada, Universidade de São Paulo, São Paulo, Brasil
- (7) Instituto Nacional de Pesquisas da Amazonia, Manaus, Amazonas, Brasil
- (8) Escola Superior de Tecnologia, Universidade do Estado do Amazonas, Manaus, Amazonas, Brasil
- (9) Atmospheric Sciences and Global Change Division, Pacific Northwest National Laboratory, Richland, WA, USA
- (10) Department of Environmental Sciences and Engineering, Gillings School of Global Public Health, The University of North Carolina at Chapel Hill, Chapel Hill, North Carolina, USA
- (11) Department of Earth and Planetary Sciences, Harvard University, Cambridge, Massachusetts, USA

<sup>a</sup> Now at Massachusetts Institute of Technology, Cambridge, Massachusetts, USA

<sup>b</sup> Now at: Laboratory for Meteorological Physics (LaMP), University Blaise Pascal, Aubière, France

<sup>\*</sup>To Whom Correspondence Should be Addressed

*E-mail: scot\_martin@harvard.edu*



1 **Abstract**

2           The atmospheric chemistry of isoprene contributes to the production of a substantial mass  
3 fraction of the particulate matter (PM) over tropical forests. Isoprene epoxydiols (IEPOX)  
4 produced in the gas phase by the oxidation of isoprene under HO<sub>2</sub>-dominant conditions are  
5 subsequently taken up by particles, thereby leading to production of secondary organic PM. The  
6 present study investigates possible perturbations to this pathway by urban pollution. The  
7 measurement site in central Amazonia was located 4 to 6 hours downwind of Manaus, Brazil.  
8 Measurements took place from February through March 2014 of the wet season, as part of the  
9 GoAmazon2014/5 experiment. Mass spectra of organic PM collected with an Aerodyne Aerosol  
10 Mass Spectrometer were analyzed by positive-matrix factorization. One resolved statistical  
11 factor (“IEPOX-SOA factor”) was associated with PM production by the IEPOX pathway.  
12 Loadings of this factor correlated with independently measured mass concentrations of tracers of  
13 IEPOX-derived PM, namely C<sub>5</sub>-alkene triols and 2-methyltetrols ( $R = 0.96$  and  $0.78$ ,  
14 respectively). Factor loading, as well as the ratio of the factor loading to organic PM mass  
15 concentration, decreased under polluted compared to background conditions. For the study  
16 period, sulfate concentration explained 37% of the variability in the factor loading. After  
17 segregation of the data set by NO<sub>y</sub> concentration, the sulfate concentration explained up to 75%  
18 of the variability in factor loading within the NO<sub>y</sub> subsets. The sulfate-detrended IEPOX-SOA  
19 factor loading decreased by two- to three-fold for an increase in NO<sub>y</sub> concentration from 0.5 to 2  
20 ppb. The suppressing effects of elevated NO dominated over the enhancing effects of higher  
21 sulfate with respect to the production of IEPOX-derived PM. Relative to background conditions,  
22 the Manaus pollution contributed more significantly to NO<sub>y</sub> than to sulfate. In this light,  
23 increased emissions of nitrogen oxides, as anticipated for some scenarios of Amazonian  
24 economic development, could significantly alter pathways of PM production that presently  
25 prevail over the tropical forest, implying changes to air quality and regional climate.



## 26 1. Introduction

27 Organic compounds comprise up to 90% of the mass concentration of submicron organic  
28 particulate matter (PM) over tropical forests (Kanakidou et al., 2005). Submicron PM has  
29 adverse effects on human health (Nel, 2005; Pope III and Dockery, 2006) and influences air  
30 quality and climate by scattering radiation and acting as cloud condensation nuclei (Ramanathan  
31 et al., 2001; Kaufman et al., 2002). A significant fraction of the submicron organic material  
32 originates from secondary processes, mainly by the atmospheric oxidation of volatile organic  
33 compounds (VOCs) emitted as part of natural and human activities (Zhang et al., 2007; Hallquist  
34 et al., 2009; Jimenez et al., 2009). The particle life cycle over Amazonia is in particular strongly  
35 influenced by secondary processes that produce organic PM (Martin et al., 2010a; Pöschl et al.,  
36 2010). Biogenic emissions from tropical forests are high, and environmental conditions favor  
37 photooxidation reactions. The reactive chemistry and the relative importance of pathways  
38 leading to PM production can be strongly guided by regulating species, such as sulfate and nitric  
39 oxide (Surratt et al., 2007a; Worton et al., 2013; Liu et al., 2016a). The concentrations of these  
40 species depend on their background occurrence, pollution sources, and the relative mix of  
41 background and polluted air masses.

42 Over tropical forests such as Amazonia, the atmospheric chemistry of isoprene produces  
43 a substantial fraction of the submicron organic PM (Chen et al., 2009; Robinson et al., 2011;  
44 Chen et al., 2015; Isaacman-VanWertz et al., 2016). Isoprene (2-methyl-1,3-butadiene,  $C_5H_8$ ) is  
45 the non-methane VOC most abundantly emitted by tropical forests (Guenther et al., 2012), and  
46 isoprene epoxydiols (IEPOX) have been identified as important intermediates in the production  
47 of PM from isoprene (Paulot et al., 2009; Surratt et al., 2010; Lin et al., 2012). A chemical  
48 sequence for the production of IEPOX-derived PM from the photooxidation of isoprene in the



49 atmosphere is represented in Figure 1. The sequence is initiated when isoprene peroxy radicals  
50 (ISOPOO) are produced in the gas phase by reactions between isoprene and photochemically  
51 generated hydroxyl radicals (OH). The reactive fate of the ISOPOO radicals can differ under  
52 background compared to polluted conditions (Surratt et al., 2010; Crounse et al., 2011; Worton et  
53 al., 2013).

54 Under background conditions, meaning that HO<sub>2</sub> pathways are favorable in the absence  
55 of extensive NO pollution (Wennberg, 2013; Liu et al., 2016a), the ISOPOO radicals continue in  
56 large part through the series of species highlighted in yellow in Figure 1. Through HO<sub>x</sub>-  
57 facilitated reaction steps, the ISOPOO radicals produce hydroperoxides (ISOPOOH) as major  
58 first-generation products and subsequently isoprene epoxydiols (IEPOX) as major second-  
59 generation products (Carlton et al., 2009; Paulot et al., 2009; Liu et al., 2013; St. Clair et al.,  
60 2015; Liu et al., 2016a). Some of the produced IEPOX undergoes reactive uptake to particles, as  
61 facilitated by hydronium ions at the surface (Surratt et al., 2007a; Lin et al., 2012; Gaston et al.,  
62 2014; Kuwata et al., 2015; Lewandowski et al., 2015). This chemical sequence can contribute a  
63 significant fraction of submicron PM mass concentration over tropical forests (Claeys et al.,  
64 2004; Hu et al., 2015). Laboratory studies indicate that about half of the PM produced by  
65 isoprene photooxidation under HO<sub>2</sub>-dominant conditions in the presence of acidic sulfate  
66 particles is associated with IEPOX production and uptake (Liu et al., 2015). Interaction of  
67 IEPOX with cloud waters warrants investigation (Lim et al., 2005; Ervens et al., 2011;  
68 Budisulistiorini et al., 2015; Chen et al., 2015). In addition to IEPOX pathways, laboratory  
69 studies suggest that multifunctional hydroperoxides produced in the gas phase can contribute to  
70 isoprene-derived PM production (Krechmer et al., 2015; Liu et al., 2016b; Riva et al., 2016b).



71           After reactive uptake of IEPOX, particle-phase reactions can produce several different  
72 families of species. These species are collectively labeled “IEPOX-derived PM” and represent a  
73 subset of the ambient organic PM, as labeled in Figure 1. The presence of 2-methyltetrols, C<sub>5</sub>-  
74 alkene triols, 3-methyltetrahydrofuran-3,4-diols, organosulfates, and related oligomers in  
75 ambient PM is an indicator of PM production by IEPOX uptake under atmospheric conditions  
76 (Claeys et al., 2004; Surratt et al., 2006; Surratt et al., 2007b; Surratt et al., 2010; Robinson et al.,  
77 2011; Lin et al., 2012; Lin et al., 2014). Even though these species may differ in some cases from  
78 the actual compounds in the atmospheric PM due to thermal decomposition during analysis  
79 (Lopez-Hilfiker et al., 2016), they serve as chemical tracers for the atmospheric concentration of  
80 IEPOX-derived PM (Hu et al., 2015; Isaacman-VanWertz et al., 2016). The analytical methods  
81 highlighted in Figure 1, including that of the “IEPOX-SOA factor” of the AMS analysis used  
82 herein, can lead to over- and underestimated IEPOX-derived PM concentrations. This  
83 uncertainty is represented in the figure by the brown dashed lines that approximately but not  
84 exactly correspond to IEPOX-derived PM.

85           Under polluted conditions, the reactive sequence of isoprene and ultimately PM  
86 production can become significantly altered (Figure 1). NO concentrations can be sufficiently  
87 high that ISOPOO radicals react almost entirely with NO in place of HO<sub>2</sub>, thereby largely  
88 producing methacrolein (MACR) and methyl vinyl ketone (MVK) in place of ISOPOOH (Liu et  
89 al., 2016a). As a result, IEPOX production can be greatly decreased, ultimately reducing PM  
90 production by IEPOX pathways. A minor channel along the NO pathway can still produce  
91 IEPOX, although much less efficiently (Jacobs et al., 2014). Under NO-dominant conditions,  
92 alternative pathways of PM production can become active, though in lower yields. MACR can be  
93 oxidized to produce peroxyacetyl nitric anhydride (MPAN), which is a precursor to



94 methacrylic acid epoxide (MAE) and hydroxymethylmethyl- $\alpha$ -lactone (HMML), and these  
95 compounds can undergo reactive uptake to produce PM (Kjaergaard et al., 2012; Lin et al., 2013;  
96 Worton et al., 2013; Nguyen et al., 2015). Glyoxal produced from isoprene oxidation can  
97 contribute to PM production (Volkamer et al., 2007; Ervens and Volkamer, 2010; McNeill et al.,  
98 2012; Marais et al., 2016).

99 Another possible mechanism affecting PM production by IEPOX uptake under polluted  
100 conditions is altered particle composition, especially particle acidity, largely driven by sulfate.  
101 Laboratory studies show that IEPOX uptake increases with increasing acidity (Gaston et al.,  
102 2014; Kuwata et al., 2015; Liu et al., 2015). A proposed reaction during uptake is the acid-  
103 catalyzed ring opening of the IEPOX molecule (Surratt et al., 2010). The subsequent particle-  
104 phase reactions include the addition of available nucleophiles, such as water to produce tetrols or  
105 sulfate to produce organosulfates as well as their oligomers (Surratt et al., 2010; Lin et al., 2014;  
106 Nguyen et al., 2014). In support of this proposed mechanism, analyses by positive-matrix  
107 factorization (PMF) of mass spectra collected in the southeastern USA identified PMF factors  
108 associated with IEPOX-derived PM, and these factors correlated positively with sulfate mass  
109 concentrations (Budisulistiorini et al., 2013; Hu et al., 2015; Xu et al., 2015). In short, different  
110 regimes of NO:HO<sub>2</sub> concentration ratios and different possible PM compositions between  
111 polluted and background conditions can lead to different product distributions and different  
112 production rates of IEPOX-derived PM.

113 The extent to which pollution may shift the production pathways of IEPOX-derived PM  
114 over tropical forests remains to be elucidated. The study described herein is based on data sets  
115 collected in the wet season downwind of Manaus, Brazil, during the *Observations and Modeling*  
116 *of the Green Ocean Amazon* Experiment (GoAmazon2014/5) (Martin et al., 2016c). The research



117 site was influenced at times and to variable extents by the pollution outflow from the Manaus  
118 metropolitan area. Compared to the background environment in Amazonia, the Manaus plume  
119 had high number concentrations of particles and enhanced concentrations of pollutants, including  
120 oxides of nitrogen and sulfate (Kuhn et al., 2010; Martin et al., 2016c). The reactive gas-phase  
121 chemistry was strongly guided by the relative mix of background and polluted air masses (Trebs  
122 et al., 2012; Liu et al., 2016a). The analysis herein focuses on how the pollution perturbed  
123 IEPOX-derived PM production relative to background conditions.

## 124 **2. Methodology**

125 Data sets were collected at the “T3” site (3.2133 °S, 60.5987 °W) located 70 km to the  
126 west of Manaus, Brazil, in central Amazonia (Martin et al., 2016c). The site was situated in a  
127 pasture (2.5 km × 2 km) surrounded by forest. The analysis herein focuses on data sets collected  
128 during the wet season period of February 1 to March 31, 2014, corresponding to the first  
129 Intensive Operating Period (IOP1) of the GoAmazon2014/5 experiment.

130 A High-Resolution Time-of-Flight Aerosol Mass Spectrometer (HR-ToF-AMS, hereafter  
131 AMS; Aerodyne, Inc., Billerica, Massachusetts, USA) recorded the primary data set of this  
132 study. The AMS provided quantitative bulk characterization of atmospheric PM at a time  
133 resolution of minutes. The design principles and capabilities of this instrument are described in  
134 the literature (DeCarlo et al., 2006; Canagaratna et al., 2007). The instrument was housed within  
135 a temperature-controlled research container, and the inlet to the instrument sampled from 5 m  
136 above ground level. Detailed aspects of AMS operation are presented in the Supplement (Section  
137 S1). In brief, ambient measurements were obtained for every 4 of 8 min. Organic, sulfate,  
138 ammonium, nitrate, and chloride PM mass concentrations were obtained from “V-mode” data.  
139 The choice of ions to fit was aided by the “W-mode” data, which were collected once every five



140 days. Data analysis was performed using *SQUIRREL* (1.56D) and *PIKA* (1.14G) of the AMS  
141 software suite.

142 Positive-matrix factorization was applied to the time series of the organic component of  
143 the high-resolution mass spectra (Ulbrich et al., 2009). The present study focuses on one of the  
144 resolved statistical factors, referred to as the “IEPOX-SOA factor” (Hu et al., 2015). Diagnostics  
145 of the PMF analysis, especially as related to the resolved IEPOX-SOA factor, are presented in  
146 the Supplement (Section S2). A separate account is forthcoming to present the other PMF factors  
147 (de Sá, in preparation). Herein, factor profile and loading refer to the mathematical products of  
148 the multivariate statistical analysis, whereas mass spectrum and mass concentration refer to  
149 measurements.

150 In complement to the AMS data sets, mass concentrations of molecular and tracer organic  
151 species were measured using a Semi-Volatile Thermal Desorption Aerosol Gas Chromatograph  
152 (SV-TAG) at a time resolution of one hour. The instrument collected gas and particle samples,  
153 followed by thermal desorption, derivatization, and gas chromatography coupled to mass  
154 spectrometry (Isaacman et al., 2014). A summary of operational details for GoAmazon2014/5 is  
155 presented in the Supplement (Section S1), and the main account is presented in Isaacman-  
156 VanWertz et al. (2016).

157 Additional data sets used in the analysis were collected at the T3 site by instruments  
158 housed in the research container of the Mobile Aerosol Observing System (MAOS) of the ARM  
159 Climate Research Facility (ACRF) operated by the USA Department of Energy (Mather and  
160 Voyles, 2013; Martin et al., 2016c). A temperature-controlled inlet was mounted at 10 m above  
161 ground level. Measurements of nitrogen oxides were made using a chemiluminescence-based  
162 instrument (Air Quality Design). The measured odd-nitrogen family “NO<sub>y</sub>”, meaning NO<sub>x</sub> +





163 reservoir species, included NO, NO<sub>2</sub>, HNO<sub>3</sub>, organonitrates, particle nitrate, and peroxyacetyl  
164 nitrates. Further details of the NO<sub>y</sub> measurements are presented in the Supplement (Section S1).  
165 Ozone concentrations were measured by an Ozone Analyzer (Thermo Fisher, model 49i).  
166 Particle number concentrations were measured by a Condensation Particle Counter (TSI, model  
167 3772). Meteorological variables provided by the ARM Mobile Facility (AMF-1), which was also  
168 part of the ACRF, included wind direction, solar irradiance, and precipitation rate. Measurements  
169 of NO<sub>y</sub> and particle number concentration onboard the G-1 aircraft of the ARM Aerial Facility  
170 (AAF) were also used in the analysis (Schmid et al., 2014; Martin et al., 2016c).

### 171 **3. Results and Discussion**

172 The organization of the presentation herein is as follows. The factor obtained from AMS  
173 PMF analysis is presented (Section 3.1), a case study comparing background to polluted  
174 conditions is discussed (Section 3.2), the roles of sulfate (Section 3.3) and nitric oxide (Section  
175 3.4) in affecting factor loading are explored, and the influence of NO on production and loss  
176 processes of IEPOX-derived PM is considered (Section 3.5).

#### 177 **3.1 Statistical IEPOX-SOA factor**

178 Positive-matrix factorization was carried out on the time series of AMS organic mass  
179 spectra. One statistical factor had a similar pattern of peak intensities as the “IEPOX-SOA  
180 factor” identified in other studies (Figure S1) (Robinson et al., 2011; Slowik et al., 2011;  
181 Budisulistiorini et al., 2013; Budisulistiorini et al., 2015; Chen et al., 2015; Xu et al., 2015). The  
182 Pearson correlation coefficient  $R$  between this factor and one obtained for a data set in the 2008  
183 wet season in central Amazonia as part of the AMAZE-08 experiment was 0.99 (Chen et al.,  
184 2015). The ratio  $f$  of the factor loading to the mass concentration of submicron organic PM for  
185 the present study was  $0.17 \pm 0.09$  (mean  $\pm$  standard deviation). The IEPOX-SOA factor has been



186 identified previously over the maritime tropical forest of Borneo ( $f = 0.23$ ) (Robinson et al.,  
187 2011), in a rural area in Canada 70 km north of Toronto ( $f = 0.17$ ) (Slowik et al., 2011), across  
188 several locations in the summertime southeastern USA ( $f = 0.17$  to 0.41) (Budisulistiorini et al.,  
189 2013; Budisulistiorini et al., 2015; Hu et al., 2015; Xu et al., 2015; Budisulistiorini et al., 2016;  
190 Marais et al., 2016), and in AMAZE-08 ( $f = 0.34$ ) (Chen et al., 2015).

191 The IEPOX-SOA factor reported herein had prominent peaks at  $m/z$  53.04 and  $m/z$  82.04  
192 (Figure S1). The ion at  $m/z$  82.04, corresponding to  $C_5H_6O^+$ , has been attributed to 3-methylfuran  
193 (3-MF). The thermal degradation of isoprene-derived PM upon mass spectral analysis was  
194 suggested as the source of 3-MF (Robinson et al., 2011). Lin et al. (2012) proposed that  
195 sequential dehydrations upon mass spectral analysis of 3-methyltetrahydrofuran-3,4-diols, which  
196 are an identified component of IEPOX-derived PM, can produce 3-MF. Other IEPOX-derived  
197 species as well as non-IEPOX species might also contribute to the production of  $C_5H_6O^+$  ions  
198 (Surratt et al., 2010; Hu et al., 2015; Liu et al., 2016c).

199 Laboratory studies show that a mass spectrum having a pattern of peak intensities similar  
200 to that of the IEPOX-SOA factor is produced both by the uptake of IEPOX into aqueous acidic  
201 sulfate particles as well as by the photooxidation of isoprene under  $HO_2$ -dominant conditions in  
202 the presence of acidic sulfate particles (Budisulistiorini et al., 2013; Nguyen et al., 2014; Kuwata  
203 et al., 2015; Liu et al., 2015). The possibility of similar uptake by a broader range of liquid media  
204 remains to be fully tested, such as other acidic solutions as well as cloud waters. Compared to the  
205 laboratory spectra of (Liu et al., 2015), representing about 4 h of OH exposure at atmospheric  
206 concentrations ( $1.7 \times 10^6$  molec  $cm^{-3}$ ), the main difference was the relative intensity of the  $m/z$   
207 44 peak. For the IEPOX-SOA factor of the present study, this peak was four times more intense



208 (Figure S1), suggesting that the atmospheric PM was more oxidized. Hu et al. (2016) showed  
209 that heterogeneous aging of IEPOX-SOA can result in increased relative signal at  $m/z$  44.

210 By contrast, laboratory studies show that a significantly different mass spectrum from  
211 that of the IEPOX-SOA factor is obtained for PM produced from isoprene photooxidation in the  
212 absence of aqueous particles (Krechmer et al., 2015; Kuwata et al., 2015). Under these  
213 conditions, chemical pathways other than IEPOX uptake into a liquid medium appear to be  
214 active, such as the condensation of low-volatility, multifunctional compounds produced by  
215 additional oxidation of ISOPOOH (Krechmer et al., 2015; Liu et al., 2016b; Riva et al., 2016b).  
216 This non-IEPOX pathway, however, is not expected to contribute a large fraction of the  
217 produced PM during the study period because of the high RH conditions in Amazonia and the  
218 prevalence of liquid particles for the prevailing atmospheric conditions (Bateman et al., 2016; de  
219 Sá, in preparation).

220 The SV-TAG measurements of the concentrations of C<sub>5</sub>-alkene triols and 2-methyltetrols  
221 support the interpretation of the IEPOX-SOA factor as an indicator that PM was being produced,  
222 at least in significant part, from the reactive uptake of IEPOX (Claeys et al., 2004; Wang et al.,  
223 2005; Surratt et al., 2010). The factor loading strongly correlated with the concentrations of C<sub>5</sub>-  
224 alkene triols ( $R = 0.96$ ) and 2-methyltetrols ( $R = 0.78$ ) (Figure 2). These species have been  
225 associated with the IEPOX reaction pathway in several laboratory studies (Surratt et al., 2010;  
226 Riedel et al., 2016). The  $R$  value with respect to C<sub>5</sub>-alkene triols was independent of the  $f_{peak}$   
227 value of the PMF solution, demonstrating the robustness of the relative time trend of factor  
228 loading even though the factor profile and absolute loadings changed across  $f_{peak}$  values (Figure  
229 S2d).



230           The loading of the IEPOX-SOA factor may be an overestimate or an underestimate of the  
231 atmospheric concentration of the IEPOX-derived PM (Supplement, Section S2). The IEPOX-  
232 SOA factor can be understood as the net result of (i) produced IEPOX-derived PM, (ii) less that  
233 portion of the carbon that gets further oxidized and mixed into other PMF factors, and (iii) plus  
234 that portion of non-IEPOX-derived PM that gives rise to a similar AMS mass spectral pattern as  
235 the IEPOX-derived PM (Supplement, Section S2). Processes of type ii contribute to  
236 underestimates and processes of type iii lead to overestimates when using IEPOX-SOA factor  
237 loading as a surrogate for IEPOX-derived PM concentration. These uncertainties are  
238 qualitatively represented in Figure 1 by the brown dashed lines that enclose the fraction of  
239 particle material statistically captured by the factor analysis. The further analysis herein is based  
240 on using the loading of the IEPOX-SOA factor as a scalar proxy for the mass concentration of  
241 IEPOX-derived PM in a sampled air mass.

### 242 **3.2 Background compared to polluted conditions**

243           Under background conditions in the wet season, remote areas of the Amazon forest  
244 constitute one of the least polluted continental regions on Earth (Martin et al., 2010a). Nitric  
245 oxide (NO) concentrations characteristic of central Amazonia range from 20 to 70 ppt (Torres  
246 and Buchan, 1988; Bakwin et al., 1990; Levine et al., 2015). Daytime maximum ozone  
247 concentrations are 10 to 15 ppb (Rummel et al., 2007). Sulfate mass concentrations associated  
248 with in-basin processes are on average  $< 0.1 \mu\text{g m}^{-3}$ , and total background sulfate concentrations  
249 contributed by in- and out-of-basin processes rarely exceed  $0.5 \mu\text{g m}^{-3}$  (Andreae et al., 1990;  
250 Chen et al., 2009).

251           In the wet season, Manaus emissions were the most important anthropogenic influence on  
252 observations at the T3 research site (Martin et al., 2016a). The afternoons of March 3 and 13,



253 2014, are presented herein as representative cases of background and polluted conditions,  
254 respectively. Both days were sunny, and major precipitation events were absent. Particle number  
255 concentrations measured onboard the G-1 aircraft within the atmospheric boundary layer show  
256 the position of the pollution plume on these two afternoons (Figure 3).  $\text{NO}_y$  concentrations  
257 measured during the same flight are shown in Figure S3. The visualization in Figure 3 shows that  
258 on March 3 the Manaus plume passed south of the T3 site. By comparison, on March 13 the  
259 central portion of the plume passed over T3. Aircraft-based observations to track the Manaus  
260 plume were available for 16 afternoons of the two-month study period. Ground site diagnostics  
261 of the urban pollution reaching the T3 site were therefore also needed.

262 Measurements at ground level at the T3 site are plotted in Figure 4 for the afternoons of  
263 March 3 (left panel) and March 13 (right panel). Based on wind speeds, the research site was 4 to  
264 6 h downwind of Manaus (Martin et al., 2016c). Anthropogenic-biogenic interactions affecting  
265 the production of IEPOX-derived PM were driven in large part by atmospheric photochemistry  
266 at daybreak. Morning urban emissions followed by atmospheric processing arrived at the T3 site  
267 during the local afternoon. The afternoon period, in addition to the connection to the Manaus  
268 plume, was also characterized by reduced variability in other possible confounding variables,  
269 such as temperature, radiation, and relative humidity. Figure 4 shows that on the afternoon of  
270 March 3 ozone concentrations were below 10 ppb, particle number concentrations were below  
271  $1000 \text{ cm}^{-3}$ ,  $\text{NO}_y$  concentrations were less than 1 ppb, and sulfate concentrations were 0.3 to 0.4  
272  $\mu\text{g m}^{-3}$ . Species concentrations were stable throughout the afternoon. On March 13, ozone  
273 concentrations exceeded 30 ppb for most of the afternoon, particle concentrations reached 10,000  
274  $\text{cm}^{-3}$ ,  $\text{NO}_y$  concentrations consistently exceeded 1 ppb, and sulfate concentrations were 0.3 to 0.6



275  $\mu\text{g m}^{-3}$ . Concentrations fluctuated markedly throughout the afternoon on March 13, reflecting  
276 different levels of pollution influence in the air passing over the T3 site during that period.

277 Elevated concentrations of ozone, particle number, and  $\text{NO}_y$  were reliable markers of  
278 pollution influence over the course of the study period (Supplement, Section S3). Pollution was  
279 associated with stronger relative enhancements in  $\text{NO}_y$  concentrations than in sulfate  
280 concentrations (Sections 3.3 and 3.4). With respect to the IEPOX-SOA factor, Figure 4 shows  
281 that the absolute and relative loadings decreased for the polluted compared to background  
282 conditions. Relative loadings are expressed by the ratio  $f$  of IEPOX-SOA factor loading to the  
283 organic PM mass concentration. Decreased absolute and relative factor loadings under polluted  
284 conditions, presented in Figure 4 as a case study, also characterized the data sets of the entire  
285 study period. Other examples are presented in the Supplement (Figure S4).

### 286 **3.3 Sulfate as a driver of IEPOX-derived PM production**

287 A scatter plot between sulfate mass concentrations and IEPOX-SOA factor loadings for  
288 all afternoon periods is shown in Figure 5a. Background and polluted conditions are represented  
289 in the data set. For further visualization, the data set was organized into six subsets based on  
290 sulfate concentration. The medians and the means of the subsets are plotted in the figure. The  
291 visualization shows that sulfate concentration served as a first-order predictor of the IEPOX-  
292 SOA factor loading in central Amazonia in the wet season. The explanation can be a  
293 combination of increased acidity, greater reaction volume including by enhanced hygroscopic  
294 growth, and possibly a nucleophilic role for sulfate (Xu et al., 2015; Marais et al., 2016). An  
295 analysis of the relative importance of each is out of the scope of the present study (Supplement,  
296 Section S4).



297 For Figure 5a, the coefficient  $R^2$  of determination between sulfate mass concentration and  
298 factor loading was 0.37, meaning that 37% of the variance of the IEPOX-SOA factor loading  
299 was explained by sulfate mass concentration. As a point of comparison,  $R^2$  varied between 0.4  
300 and 0.6 for observations in the southeastern USA, which seasonally is a region of high isoprene  
301 emissions (Budisulistiorini et al., 2013; Budisulistiorini et al., 2015; Hu et al., 2015; Xu et al.,  
302 2015). A chemical transport model that predicted IEPOX-derived PM mass concentrations for  
303 the southeastern USA obtained  $R^2$  of 0.4 for the relationship to predicted sulfate mass  
304 concentration (Marais et al., 2016). The model attributed the correlation to the acidity and  
305 particle volume provided by sulfate, both of which favored IEPOX uptake. Central Amazonia  
306 and the southeastern USA differ considerably in terms of meteorology, chemistry, and levels of  
307 regional pollution, yet they have in common an important role of sulfate concentration as a  
308 predictor of IEPOX-derived PM concentration, even as the sulfate concentrations themselves  
309 differ by an order of magnitude. Sulfate concentrations typically had an interquartile range of  
310  $[1.5, 3.0] \mu\text{g m}^{-3}$  in the studies in the southeastern USA, which can be compared to a range of  
311  $[0.11, 0.36] \mu\text{g m}^{-3}$  under background conditions during the wet season in central Amazonia.

312 A key difference between the southeastern USA and central Amazonia is the role of  
313 sulfate concentration as a clear or ambiguous indicator, respectively, of urban influence. For the  
314 relatively low sulfate mass concentrations ( $<0.5 \mu\text{g m}^{-3}$ ) characteristic of the study period,  
315 background air in central Amazonia contributed significantly to the variability in sulfate  
316 concentration measured at the T3 site. Background concentrations of sulfate in Amazonia,  
317 distinguished from sulfate tied to the urban Manaus plume, originated from in-basin emissions of  
318 dimethyl sulfide (DMS) and hydrogen sulfide ( $\text{H}_2\text{S}$ ) from the forest as well as from out-of-basin  
319 marine emissions from the Atlantic Ocean (Andreae et al., 1990; Chen et al., 2009; Martin et al.,



320 2010a). In the wet season, biomass burning from Africa and to a lesser extent from South  
321 America also episodically contributed significantly to sulfate concentrations in the Manaus  
322 region. In addition, emissions from large cities on the eastern coast of Brazil were important at  
323 times when rare meteorological events shifted the northeasterlies typical of the wet season to  
324 easterlies (Martin et al., 2016a). Manaus contributions to sulfate mass concentrations in an air  
325 mass were in addition to these various background sources.

326 The relative importance of Manaus contributions to the sulfate concentrations in the air  
327 masses that passed over T3 was assessed by comparison of the probability density function of  
328 sulfate concentration at T3 to those of sites upwind of Manaus (Figure 5b). The distributions of  
329 the two upwind sites had a central tendency of 0.05 to 0.3  $\mu\text{g m}^{-3}$ , suggesting the range of natural  
330 concentrations, and a rightside skewness up to 0.6  $\mu\text{g m}^{-3}$ , suggesting the importance of episodic  
331 long-range transport (Chen et al., 2009). The figure shows that the distribution at T3 did not  
332 differ greatly from those of the upwind sites even though the air masses over T3 regularly  
333 transported Manaus pollution, indicating that Manaus did not constitute a dominant sulfate  
334 source in the region. Elevated sulfate concentrations on any one afternoon at the T3 site might  
335 have arisen because of elevated background concentrations on that day rather than the influence  
336 of the Manaus pollution plume. The implications are that (i) sulfate concentration was an  
337 ambiguous indicator of urban influence at the T3 site and (ii) increases in sulfate concentrations  
338 in pollution events were moderate relative to background concentrations.

### 339 **3.4 NO as a modulator of IEPOX-derived PM production**

340 In the transport from Manaus to the T3 research site, NO concentration is not conserved,  
341 in part because of reactions with ozone and organic peroxy radicals (Martin et al., 2016a). In this  
342 case, the instantaneous NO concentrations measured at the T3 site do not directly provide





343 information about the fate of ISOPOO radicals along the transport time of 4 to 6 h from Manaus  
344 to the T3 site. The collective contributions of NO, NO<sub>2</sub>, and their oxidation products are,  
345 however, reflected in measurements of NO<sub>y</sub> concentrations at the T3 site. The NO<sub>y</sub> family is  
346 expected to have a longer lifetime than the transport time from Manaus to the T3 site (Romer et  
347 al., 2016). The NO<sub>y</sub> concentration measured at T3 therefore served as a surrogate for the  
348 integrated exposure of the airmass to NO chemistry between Manaus and T3 (Liu et al., 2016a).

349 Unlike the ambiguity associated with the sulfate concentration, an elevated NO<sub>y</sub>  
350 concentration served as a clear indicator of anthropogenic influence in an air mass passing over  
351 the T3 site. For background conditions over the forest, NO<sub>y</sub> originated from NO emitted from  
352 soils and other natural sources such as lightning (Bakwin et al., 1990; Jacob and Wofsy, 1990).  
353 The probability density function of NO<sub>y</sub> concentration under background conditions in the wet  
354 season of the central Amazon basin is shown in Figure 6b (Bakwin et al., 1990). The distribution  
355 for measurements at T3 is also shown. Relative to the narrow distribution around 0.5 ppb for  
356 background conditions, there is high-side skewness extending up to 4 ppb for the T3  
357 measurements, indicating the clear influence of Manaus emissions on NO<sub>y</sub> concentrations.

358 NO<sub>y</sub> concentration was incorporated into the analysis by segregation of the dataset of  
359 Figure 5a into five subsets (Supplement, Section S5). Linear fits to the NO<sub>y</sub>-segregated data  
360 subsets are plotted in Figure 6a. Each subset is represented by a different color. Parameter values  
361 of the associated fits are listed in Table 1. In conjunction with sulfate concentration, the  
362 visualization presented in Figure 6a shows that NO<sub>y</sub> concentration further explained the  
363 variability in IEPOX-SOA factor loadings. The  $R^2$  values, representing the extent to which  
364 sulfate was able to explain variability in IEPOX-SOA factor loading once isolated for NO<sub>y</sub>  
365 concentration, were higher for the data subsets having lower and higher extremes of NO<sub>y</sub>



366 concentrations (Table 1). These conditions represent the limiting cases of fully background  
367 conditions for the former and the strongest effects of Manaus pollution for the latter. By  
368 comparison, intermediate  $\text{NO}_y$  concentrations could arise from air masses that mixed together  
369 background air with Manaus pollution during the transport to T3 (e.g., by entrainment) and thus  
370 represent complex processing. Single or multiple mixing points could occur anywhere along the  
371 path from Manaus to T3, thus introducing variability into the effective photochemical age of the  
372 air mass arriving at T3 and resulting in lower  $R^2$  values for intermediate  $\text{NO}_y$  concentrations. In  
373 caveat, this explanation assumes that NO emissions from Manaus had low day-to-day variability.

374 In relation to the influence of Manaus pollution, sulfate concentration was affected by a  
375 mixture of background and urban sources whereas  $\text{NO}_y$  concentration largely had urban sources.  
376 As an approximation to keeping the sulfate concentration constant and thus focusing on the role  
377 of NO in the urban pollution, the visualization of the dependence of IEPOX-SOA factor loading  
378 on  $\text{NO}_y$  concentration was further refined by taking data subsets segregated by low ( $< 0.1 \mu\text{g}$   
379  $\text{m}^{-3}$ ) and high ( $> 0.3 \mu\text{g m}^{-3}$ ) sulfate concentrations. Figures 7a, 7b, and 7c show the factor  
380 loading, organic PM mass concentration, and the ratio  $f$  of the IEPOX-SOA factor loading to the  
381 organic PM mass concentration, respectively, plotted against  $\text{NO}_y$  concentration for low and high  
382 sulfate concentrations.

383 Figure 7a shows that for both low and high sulfate concentrations an increase in  $\text{NO}_y$   
384 concentration from background to polluted concentrations was associated with a decrease in the  
385 IEPOX-SOA factor loading by two to three times. For low sulfate concentration, the interquartile  
386 range of the factor loading decreased from [0.037, 0.093] to [0.022, 0.039]  $\mu\text{g m}^{-3}$  for an increase  
387 in  $\text{NO}_y$  concentration from 0.5 to 2 ppb. For high sulfate concentration, the factor loading  
388 decreased from [0.57, 0.95] to [0.21, 0.35]  $\mu\text{g m}^{-3}$  for the same transition in  $\text{NO}_y$  concentration.



389 The greatest changes in factor loading were in the region of 1 ppb  $\text{NO}_y$ . This region of greatest  
390 sensitivity coincided with the transition from background to polluted conditions. For the same  
391 time period, a change was reported in the gas phase from a dominance of ISOPOOH to  
392 MVK/MACR products across this transition in  $\text{NO}_y$  concentration (Liu et al., 2016a).

393 Figure 7b shows that for both low and high sulfate concentrations the organic PM mass  
394 concentration  $M_{\text{org}}$  and the IEPOX-SOA factor loading had opposite trends for low compared to  
395 intermediate  $\text{NO}_y$  concentrations, even though the trend in  $M_{\text{org}}$  was less steep. The factor  
396 loadings decreased by 60% whereas the  $M_{\text{org}}$  increased by 25% for 0.5 to 2 ppb  $\text{NO}_y$  (Figures 7a  
397 and 7b). Increases in  $M_{\text{org}}$  can include contributions from secondary PM produced by enhanced  
398 concentrations of hydroxyl radicals and ozone in the pollution plume as well as from primary  
399 PM emitted from the Manaus urban region (Martin et al., 2016a; de Sá, in preparation). For  
400 higher  $\text{NO}_y$  concentrations (> 2 ppb), however, Figure 7b shows that  $M_{\text{org}}$  decreased after a peak  
401 value, approaching values close to background under the most polluted conditions. The  
402 chemistry can become sufficiently shifted that more-volatile gas-phase products can be produced  
403 (Pandis et al., 1991; Kroll et al., 2005; Carlton et al., 2009). In addition, hydroxyl radical  
404 concentrations can also decrease because of titration by  $\text{NO}_2$  (Valin et al., 2013; Rohrer et al.,  
405 2014). An increase in total organic mass concentration could possibly contribute to a decrease in  
406 IEPOX-derived PM production by kinetically limiting the uptake of IEPOX (Gaston et al., 2014;  
407 Lin et al., 2014; Riva et al., 2016a). The dominant effect of the urban plume, however, seems to  
408 be that of shifting the fate of ISOPOO radicals through the increase in  $\text{NO}$ , thereby significantly  
409 decreasing the production of ISOPOOH (Liu et al., 2016a) (Section 3.5).

410 The combined trends of Figures 7a and 7b for increasing  $\text{NO}_y$  are represented in Figure  
411 7c as the ratio  $f$ . The figure shows that  $f$  decreased for increasing  $\text{NO}_y$  concentration for both low



412 and high sulfate concentrations. The greatest decrease occurred across the range of  $\text{NO}_y$   
413 concentrations that represented the shift from background to polluted conditions. For low sulfate  
414 concentration, the interquartile range of  $f$  decreased from [0.09, 0.18] to [0.04, 0.09] for an  
415 increase in  $\text{NO}_y$  concentration from 0.5 to 2 ppb. These ranges shifted to [0.35, 0.40] and [0.07,  
416 0.18] for high sulfate concentration. The magnitude of the decrease for high sulfate  
417 concentrations suggests that IEPOX-derived PM shifted from being a major to a minor  
418 component of the PM, although the caveats related to under- and overestimates connected to the  
419 IEPOX-SOA factor should be kept in mind (vide supra). Taken together, the results shown in  
420 Figure 7 demonstrate how urban pollution affected the production and composition of regional  
421 IEPOX-derived PM.

422 The data sets presented in Figures 5, 6, and 7 lead to the conclusion that the additional  
423  $\text{NO}$  concentrations contributed by Manaus emissions typically suppress the production of  
424 IEPOX-derived PM to a greater extent than the additional sulfate concentrations enhance it.  
425 Figure 8 presents a systematic visualization. The factor loadings at T3 are represented as  
426 contours for axes of sulfate and  $\text{NO}_y$  concentrations. Higher factor loadings are favored for  
427 higher sulfate and lower  $\text{NO}_y$  concentrations. Factor loadings are most sensitive to changing  
428 concentration in the high-sulfate, low- $\text{NO}_y$  region. The gray dashed line in Figure 8 represents a  
429 qualitative divisor between domains of typical background and polluted conditions downwind of  
430 Manaus.

### 431 **3.5 Influence of $\text{NO}$ on production and loss processes of IEPOX-derived PM**

432 Elevated  $\text{NO}$  may affect both the production and loss processes of IEPOX-derived PM.  
433 On the one hand, production may be reduced because of increased scavenging of ISOPOO by  
434  $\text{NO}$ , thus obviating production of IEPOX and consequently of IEPOX-derived PM. Production



435 may also be reduced because of more rapid gas-phase loss of IEPOX in response to elevated OH  
436 and O<sub>3</sub> concentrations. On the other hand, loss of IEPOX-derived PM may be enhanced due to  
437 faster processing of its characteristic compounds by the elevated oxidant concentrations.

438 A Lagrangian model is employed to help delineate the relative importance of reduced  
439 production compared to enhanced loss on the observed IEPOX-derived PM concentrations. The  
440 model is initialized by background air that passes over Manaus in the mid-morning. The  
441 evolution of IEPOX-derived PM in that air mass is modeled under either polluted or background  
442 conditions for arrival at the T3 site in the afternoon. The governing differential equation of the  
443 model represents the sum of production and loss processes affecting the concentrations of  
444 IEPOX-derived PM, as follows:

$$445 \quad \frac{dM}{dt} = -\alpha_L k_L M + \alpha_P k_P \quad (1)$$

446 where  $M$  designates the IEPOX-derived PM mass concentration,  $t$  designates time, and the first  
447 and second terms on the right-hand side represent loss and production processes, respectively.  
448 Table 2 lists other symbol definitions and units.

449 The analytic solution of Equation 1 for time  $t$  is presented in the Supplement (Section  
450 S6). From this solution, characteristic times  $\tau$  for production and loss processes for polluted  
451 compared to background conditions are as follows:  $\tau_{P,pol} = M_0 / (\alpha_P k_P)$ ,  $\tau_{P,bg} = M_0 / k_P$ ,  $\tau_{L,pol} = 1 /$   
452  $(\alpha_L k_L)$ , and  $\tau_{L,bg} = 1 / k_L$  (Supplement, Section S6). The term  $M_0$  represents the IEPOX-derived  
453 PM mass concentration just upwind of Manaus. Under background conditions, the enhancement  
454 factors  $\alpha_L$  and  $\alpha_P$  are unity by definition. Under polluted conditions,  $\alpha_L = 2$  and  $\alpha_P = 0.1$  to reflect  
455 enhanced loss and decreased production, respectively. Further descriptions of the model and  
456 assumptions are presented in the Supplement (Section S6).



457           The analysis strategy is to compare  $\tau_P$  and  $\tau_L$  to the transport time  $\tau_{tr}$  under polluted and  
458 background conditions to assess the relative importance of altered production and loss processes  
459 for IEPOX-derived PM from Manaus to T3. The mode value for  $\tau_{tr}$  is 4 h based on trajectory  
460 analysis (Martin et al., 2016c). Intervals for the characteristic times  $\tau_P$  and  $\tau_L$  are constrained by  
461 the T3 afternoon data sets. Concentration ratios  $\zeta$ , defined as  $\zeta = M_{pol} / M_{bg}$ , are used to constrain  
462 the model (Table 3). The quantities  $M_{pol}$  and  $M_{bg}$  denote  $M(t = \tau_{tr})$ , meaning the mass  
463 concentration at T3 under polluted or background conditions, respectively. The use of the ratio  
464 quantity  $\zeta$  in the analysis, rather than absolute concentrations, provides increased robustness  
465 because of low variability in  $\zeta$  across the observed range of sulfate concentrations, even as  $M_{pol}$   
466 and  $M_{bg}$  vary greatly (Table 3). The possible impact of over- or underestimates of IEPOX-  
467 derived PM mass concentration, as a consequence of using IEPOX-SOA factor loading as a  
468 surrogate, is also mitigated by the use of  $\zeta$ .

469           Two cases of the model (1 and 2) are presented, respectively focusing on constraining  $k_P$   
470 or  $k_L$  and consequently  $\tau_P$  or  $\tau_L$  (Table 4). The results for Case 1 of the analysis are shown in  
471 Figure 9a. The value of  $k_P$  is varied from 0 to  $0.2 \mu\text{g m}^{-3} \text{h}^{-1}$  while the other model parameters are  
472 held constant. The loss rate coefficient  $k_L$  is fixed at  $0.015 \text{ h}^{-1}$ , corresponding to a characteristic  
473 time of 2.8 days (Supplement, Section S6). Based on observed values of  $\zeta$  (gray shaded area in  
474 Figure 9a), an interval for  $k_P$  of  $[0.07, 0.13] \mu\text{g m}^{-3} \text{h}^{-1}$  is obtained, as indicated by the vertical  
475 dashed lines. Across this interval,  $M_{bg}$  and  $M_{pol}$  vary from  $0.49$  to  $0.72 \mu\text{g m}^{-3}$  and  $0.23$  to  $0.25 \mu\text{g}$   
476  $\text{m}^{-3}$ , respectively, which are consistent with the observed IEPOX-SOA factor loadings (Table 3).  
477 The modeled production times have intervals of  $[1.8, 3.3] \text{ h}$  for  $\tau_{P,bg}$  and  $[18, 33] \text{ h}$  for  $\tau_{P,pol}$ .

478           Case 2 of the analysis evaluates constraints on the loss rate coefficient  $k_L$ , and results are  
479 shown in Figure 9b. Loss processes can include chemistry, such as heterogeneous oxidation or



480 other in-particle reactions that reduce the IEPOX-SOA factor loading, as well as physical  
481 mechanisms, such as particle deposition and particle dilution by entrainment that reduce mass  
482 concentrations of IEPOX-derived PM (Supplement, Section S6). The value of  $k_L$  is varied over  
483 three orders of magnitude, representing characteristic times of hours to weeks, while the other  
484 model parameters are held constant (Table 4). The production rate coefficient  $k_P$  is fixed at 0.10  
485  $\mu\text{g m}^{-3} \text{h}^{-1}$ , corresponding to the interval midpoint of Case 1. The observed values of  $\zeta$  (gray  
486 shaded area) in intersection with the modeled values of  $\zeta$  imply an upper limit on  $k_L$  at  $0.043 \text{ h}^{-1}$ ,  
487 corresponding to characteristic times of a day to weeks (Figure 9b). Correspondingly,  $\tau_{L,bg} > 24$   
488 h under background conditions, and  $\tau_{L,pol} > 12$  h under polluted conditions.

489 The analyses of Cases 1 and 2 constrain the values of  $\tau_{P,pol}$ ,  $\tau_{P,bg}$ ,  $\tau_{L,pol}$ , and  $\tau_{L,bg}$  based on  
490 the observed values of  $\zeta$ . The lower limits of the characteristic times for loss, meaning  $\tau_{L,bg} > 24$   
491 h and  $\tau_{L,pol} > 12$  h, are considerably longer than the transport time of 4 h under both background  
492 and polluted conditions. Enhanced loss, therefore, does not explain alone the observed values of  
493  $\zeta$ . By comparison, the observed values of  $\zeta$  imply a shift in the characteristic time for production  
494 from [1.8, 3.3] h under background conditions to [18, 33] h under pollution conditions. The shift  
495 in timescale is significant in light of the transport time of 4 h. Therefore, reduced production,  
496 rather than enhanced loss, is consistent with the lower IEPOX-derived PM concentrations under  
497 polluted conditions. A few afternoon hours of altered isoprene chemistry is sufficient to  
498 significantly shift the atmospheric concentration of IEPOX-derived PM.

#### 499 **4. Summary and conclusions**

500 The influence of anthropogenic emissions on the production of organic particulate matter  
501 from isoprene epoxydiols was studied during the wet season of the tropical forest in central  
502 Amazonia. The IEPOX-derived PM concentration at the T3 site, as indicated by the IEPOX-



503 SOA factor loading, was lower under polluted compared to background conditions. Sulfate  
504 concentration was an important first-order predictor of the IEPOX-SOA factor loading,  
505 corroborating the understanding of the role of sulfate in the production of IEPOX-derived PM  
506 that has been developed in laboratory studies as well as in investigations in the southeastern USA  
507 (Surratt et al., 2007b; Budisulistiorini et al., 2013; Budisulistiorini et al., 2015; Hu et al., 2015;  
508 Kuwata et al., 2015; Xu et al., 2015). Unlike the southeastern USA, however, where  
509 anthropogenic influences dominated variability in sulfate concentrations, contributions by the  
510 Manaus urban region to sulfate concentrations were of approximately equal magnitude to the  
511 background variability in central Amazonia. By comparison, Manaus urban emissions of NO  
512 dominated over background concentrations, and the NO<sub>y</sub> concentration measured 4 to 6 h  
513 downwind of Manaus at the T3 site was an important predictor of the IEPOX-SOA factor  
514 loading. In net effect, the suppression of IEPOX production because of elevated NO  
515 concentrations in the pollution plume dominated over any enhancements in IEPOX uptake  
516 because of greater sulfate concentrations.

517         The dependence of the IEPOX-SOA factor loadings on both sulfate and NO<sub>y</sub>  
518 concentrations, as shown in Figure 8, suggests that altered net anthropogenic effects may be  
519 expected for different geographic regions, even within Amazonia, and different time periods,  
520 such as the wet and dry seasons. The T3 site experienced a wide range of NO<sub>y</sub> concentrations,  
521 allowing for the systematic demonstration of the dependence of IEPOX-derived PM  
522 concentrations on NO<sub>y</sub> concentrations. The results show that the transition in isoprene  
523 photochemistry related to the production of IEPOX-derived PM is most sensitive precisely at the  
524 transition between background and polluted conditions, around 1 ppb of NO<sub>y</sub>, at least for central  
525 Amazonia in the wet season. These findings suggest that the fraction of PM derived from IEPOX





526 might be lower and have lower variability for other geographic regions characterized by higher  
527  $\text{NO}_y$  baseline concentrations (e.g., upward of 1 to 2 ppb). For regions further downwind of the  
528 urban center, the effects of the plume are expected to phase out both due to dilution and to  
529 consumption of  $\text{NO}$ , and a gradual transition to background chemistry is expected to take place.  
530 Adequately representing background conditions and the transition to polluted conditions within  
531 models, including the dependence of the production of IEPOX-derived PM not only on sulfate  
532 but also on  $\text{NO}$  concentration, is thus important for making accurate predictions of PM  
533 concentrations, both in Amazonia and around the globe.

534         The findings herein can be considered in the context of Amazonia in transition (Davidson  
535 et al., 2012). In the past 50 years, the metropolitan area of Manaus, today at more than 2 million  
536 inhabitants, has experienced rapid economic and population growth (Martin et al., 2016c).  
537 Changes in the fuel matrix, such as the ongoing shift from high-sulfur to low-sulfur oil in the  
538 vehicle fleet as well as from fuel oil to natural gas in many power plants (Medeiros et al., in  
539 preparation), are changing the composition of the Manaus pollution plume. Based on the findings  
540 presented herein, a reduction in sulfate sources from Manaus would not be expected to  
541 considerably affect the mass concentration of IEPOX-derived species in forest regions affected  
542 by the plume. Background sources independent of Manaus appear sufficient to sustain sulfate  
543 concentrations regionally. On the other hand, in the absence of pollution control technologies,  
544  $\text{NO}$  emissions can be expected to increase in coming years due to the development of more  
545 efficient (i.e., higher temperature) sources of electricity associated with the development of  
546 natural gas resources in the basin, as well as from growth in transportation associated with  
547 increased population. Increased  $\text{NO}$  concentrations can be expected to reduce the mass  
548 concentration of IEPOX-derived species in forest regions affected by the plume. Changes in the



549 atmospheric particle population can have follow-on effects on cloud type, duration, and rainfall  
550 (Pöschl et al., 2010). In addition to PM derived from IEPOX as discussed herein, a better  
551 understanding of other pathways that also contribute to organic PM, as well as possible changes  
552 to those pathways with increasing pollution in the region, warrants further study so as to achieve  
553 sufficient knowledge for decision-making related to air quality and climate in Amazonia.



**Acknowledgments.** Institutional support was provided by the Central Office of the Large Scale Biosphere Atmosphere Experiment in Amazonia (LBA), the National Institute of Amazonian Research (INPA), and Amazonas State University (UEA). We acknowledge support from the Atmospheric Radiation Measurement (ARM) Climate Research Facility, a user facility of the United States Department of Energy (DOE), Office of Science, sponsored by the Office of Biological and Environmental Research, and support from the Atmospheric System Research (ASR) program of that office. Additional funding was provided by the Amazonas State Research Foundation (FAPEAM), the São Paulo State Research Foundation (FAPESP), the USA National Science Foundation (NSF), and the Brazilian Scientific Mobility Program (CsF/CAPES). S. de Sá acknowledges support by the Schlumberger Foundation, Faculty for the Future Fellowship. The research was conducted under scientific license 001030/2012-4 of the Brazilian National Council for Scientific and Technological Development (CNPq).



## References

- Andreae, M., Berresheim, H., Bingemer, H., Jacob, D. J., Lewis, B., Li, S. M., and Talbot, R. W.: The atmospheric sulfur cycle over the Amazon Basin: 2. Wet season, *J. Geophys. Res. Atmos.*, 95, 16813-16824, 1990, 10.1029/JD095iD10p16813.
- Andreae, M. O., Acevedo, O. C., Araùjo, A., Artaxo, P., Barbosa, C. G. G., Barbosa, H. M. J., Brito, J., Carbone, S., Chi, X., Cintra, B. B. L., da Silva, N. F., Dias, N. L., Dias-Júnior, C. Q., Ditas, F., Ditz, R., Godoi, A. F. L., Godoi, R. H. M., Heimann, M., Hoffmann, T., Kesselmeier, J., Könemann, T., Krüger, M. L., Lavric, J. V., Manzi, A. O., Lopes, A. P., Martins, D. L., Mikhailov, E. F., Moran-Zuloaga, D., Nelson, B. W., Nölscher, A. C., Santos Nogueira, D., Piedade, M. T. F., Pöhlker, C., Pöschl, U., Quesada, C. A., Rizzo, L. V., Ro, C. U., Ruckteschler, N., Sá, L. D. A., de Oliveira Sá, M., Sales, C. B., dos Santos, R. M. N., Saturno, J., Schöngart, J., Sörgel, M., de Souza, C. M., de Souza, R. A. F., Su, H., Targhetta, N., Tóta, J., Trebs, I., Trumbore, S., van Eijck, A., Walter, D., Wang, Z., Weber, B., Williams, J., Winderlich, J., Wittmann, F., Wolff, S., and Yáñez-Serrano, A. M.: The Amazon Tall Tower Observatory (ATTO): overview of pilot measurements on ecosystem ecology, meteorology, trace gases, and aerosols, *Atmos. Chem. Phys.*, 15, 10723-10776, 2015, 10.5194/acp-15-10723-2015.
- Bakwin, P. S., Wofsy, S. C., Fan, S. M., Keller, M., Trumbore, S. E., and Da Costa, J. M.: Emission of nitric oxide (NO) from tropical forest soils and exchange of NO between the forest canopy and atmospheric boundary layers, *J. Geophys. Res. Atmos.*, 95, 16755-16764, 1990, 10.1029/JD095iD10p16755.
- Bateman, A. P., Gong, Z., Liu, P., Sato, B., Cirino, G., Zhang, Y., Artaxo, P., Bertram, A. K., Manzi, A. O., Rizzo, L. V., Souza, R. A. F., Zaveri, R. A., and Martin, S. T.: Sub-



- micrometre particulate matter is primarily in liquid form over Amazon rainforest, *Nature Geosci.*, 9, 34-37, 2016, 10.1038/ngeo2599  
<http://www.nature.com/ngeo/journal/v9/n1/abs/ngeo2599.html#supplementary-information>.
- Budisulistiorini, S. H., Canagaratna, M. R., Croteau, P. L., Marth, W. J., Baumann, K., Edgerton, E. S., Shaw, S. L., Knipping, E. M., Worsnop, D. R., Jayne, J. T., Gold, A., and Surratt, J. D.: Real-time continuous characterization of secondary organic aerosol derived from isoprene epoxydiols in downtown Atlanta, Georgia, using the Aerodyne Aerosol Chemical Speciation Monitor, *Environ. Sci. Technol.*, 47, 5686-5694, 2013, 10.1021/es400023n.
- Budisulistiorini, S. H., Li, X., Bairai, S. T., Renfro, J., Liu, Y., Liu, Y. J., McKinney, K. A., Martin, S. T., McNeill, V. F., Pye, H. O. T., Nenes, A., Neff, M. E., Stone, E. A., Mueller, S., Knote, C., Shaw, S. L., Zhang, Z., Gold, A., and Surratt, J. D.: Examining the effects of anthropogenic emissions on isoprene-derived secondary organic aerosol formation during the 2013 Southern Oxidant and Aerosol Study (SOAS) at the Look Rock, Tennessee ground site, *Atmos. Chem. Phys.*, 15, 8871-8888, 2015, 10.5194/acp-15-8871-2015.
- Budisulistiorini, S. H., Baumann, K., Edgerton, E. S., Bairai, S. T., Mueller, S., Shaw, S. L., Knipping, E. M., Gold, A., and Surratt, J. D.: Seasonal characterization of submicron aerosol chemical composition and organic aerosol sources in the southeastern United States: Atlanta, Georgia, and Look Rock, Tennessee, *Atmos. Chem. Phys.*, 16, 5171-5189, 2016, 10.5194/acp-16-5171-2016.
- Canagaratna, M. R., Jayne, J. T., Jimenez, J. L., Allan, J. D., Alfarra, M. R., Zhang, Q., Onasch, T. B., Drewnick, F., Coe, H., Middlebrook, A., Delia, A., Williams, L. R., Trimborn, A.



- M., Northway, M. J., DeCarlo, P. F., Kolb, C. E., Davidovits, P., and Worsnop, D. R.: Chemical and microphysical characterization of ambient aerosols with the aerodyne aerosol mass spectrometer, *Mass Spectrom. Rev.*, 26, 185-222, 2007, 10.1002/mas.20115.
- Carlton, A., Wiedinmyer, C., and Kroll, J.: A review of secondary organic aerosol (SOA) formation from isoprene, *Atmos. Chem. Phys.*, 9, 4987-5005, 2009, 10.5194/acp-9-4987-2009.
- Chen, Q., Farmer, D. K., Schneider, J., Zorn, S. R., Heald, C. L., Karl, T. G., Guenther, A., Allan, J. D., Robinson, N., Coe, H., Kimmel, J. R., Pauliquevis, T., Borrmann, S., Pöschl, U., Andreae, M. O., Artaxo, P., Jimenez, J. L., and Martin, S. T.: Mass spectral characterization of submicron biogenic organic particles in the Amazon Basin, *Geophys. Res. Lett.*, 36, L20806, 2009, 10.1029/2009GL039880.
- Chen, Q., Farmer, D. K., Rizzo, L. V., Pauliquevis, T., Kuwata, M., Karl, T. G., Guenther, A., Allan, J. D., Coe, H., Andreae, M. O., Pöschl, U., Jimenez, J. L., Artaxo, P., and Martin, S. T.: Submicron particle mass concentrations and sources in the Amazonian wet season (AMAZE-08), *Atmos. Chem. Phys.*, 15, 3687-3701, 2015, 10.5194/acp-15-3687-2015.
- Claeys, M., Graham, B., Vas, G., Wang, W., Vermeylen, R., Pashynska, V., Cafmeyer, J., Guyon, P., Andreae, M. O., Artaxo, P., and Maenhaut, W.: Formation of secondary organic aerosols through photooxidation of isoprene, *Science*, 303, 1173-1176, 2004, 10.1126/science.1092805.
- Crouse, J. D., Paulot, F., Kjaergaard, H. G., and Wennberg, P. O.: Peroxy radical isomerization in the oxidation of isoprene, *Phys. Chem. Chem. Phys.*, 13, 13607-13613, 2011, 10.1039/C1CP21330J.



- Davidson, E. A., de Araújo, A. C., Artaxo, P., Balch, J. K., Brown, I. F., Bustamante, M. M., Coe, M. T., DeFries, R. S., Keller, M., and Longo, M.: The Amazon basin in transition, *Nature*, 481, 321-328, 2012.
- de Sá, S. S.: Sources and composition of submicron particulate matter in Amazonia as affected by anthropogenic emissions during the wet and dry season, in preparation.
- DeCarlo, P. F., Kimmel, J. R., Trimborn, A., Northway, M. J., Jayne, J. T., Aiken, A. C., Gonin, M., Fuhrer, K., Horvath, T., Docherty, K. S., Worsnop, D. R., and Jimenez, J. L.: Field-deployable, high-resolution, time-of-flight aerosol mass spectrometer, *Anal. Chem.*, 78, 8281-8289, 2006, 10.1021/ac061249n.
- Ervens, B. and Volkamer, R.: Glyoxal processing by aerosol multiphase chemistry: towards a kinetic modeling framework of secondary organic aerosol formation in aqueous particles, *Atmos. Chem. Phys.*, 10, 8219-8244, 2010, 10.5194/acp-10-8219-2010.
- Ervens, B., Turpin, B., and Weber, R.: Secondary organic aerosol formation in cloud droplets and aqueous particles (aqSOA): a review of laboratory, field and model studies, *Atmos. Chem. Phys.*, 11, 11069-11102, 2011, 10.5194/acp-11-11069-2011.
- Fu, T. M., Jacob, D. J., Wittrock, F., Burrows, J. P., Vrekoussis, M., and Henze, D. K.: Global budgets of atmospheric glyoxal and methylglyoxal, and implications for formation of secondary organic aerosols, *J. Geophys. Res. Atmos.*, 113, D15303, 2008, 10.1029/2007JD009505.
- Gaston, C. J., Riedel, T. P., Zhang, Z., Gold, A., Surratt, J. D., and Thornton, J. A.: Reactive uptake of an isoprene-derived epoxydiol to submicron aerosol particles, *Environ. Sci. Technol.*, 48, 11178-11186, 2014, 10.1021/es5034266.



Guenther, A., Jiang, X., Heald, C., Sakulyanontvittaya, T., Duhl, T., Emmons, L., and Wang, X.:

The Model of Emissions of Gases and Aerosols from Nature version 2.1 (MEGAN2. 1):  
an extended and updated framework for modeling biogenic emissions, *Geosci. Model  
Dev.*, 5, 1471–1492, 2012, 10.5194/gmd-5-1471-2012.

Hallquist, M., Wenger, J. C., Baltensperger, U., Rudich, Y., Simpson, D., Claeys, M., Dommen,  
J., Donahue, N. M., George, C., Goldstein, A. H., Hamilton, J. F., Herrmann, H.,  
Hoffmann, T., Iinuma, Y., Jang, M., Jenkin, M. E., Jimenez, J. L., Kiendler-Scharr, A.,  
Maenhaut, W., McFiggans, G., Mentel, T. F., Monod, A., Prévôt, A. S. H., Seinfeld, J.  
H., Surratt, J. D., Szmigielski, R., and Wildt, J.: The formation, properties and impact of  
secondary organic aerosol: current and emerging issues, *Atmos. Chem. Phys.*, 9, 5155-  
5236, 2009, 10.5194/acp-9-5155-2009.

Hu, W. W., Campuzano-Jost, P., Palm, B. B., Day, D. A., Ortega, A. M., Hayes, P. L.,  
Krechmer, J. E., Chen, Q., Kuwata, M., Liu, Y. J., de Sá, S. S., McKinney, K., Martin, S.  
T., Hu, M., Budisulistiorini, S. H., Riva, M., Surratt, J. D., St. Clair, J. M., Isaacman-Van  
Wertz, G., Yee, L. D., Goldstein, A. H., Carbone, S., Brito, J., Artaxo, P., de Gouw, J. A.,  
Koss, A., Wisthaler, A., Mikoviny, T., Karl, T., Kaser, L., Jud, W., Hansel, A., Docherty,  
K. S., Alexander, M. L., Robinson, N. H., Coe, H., Allan, J. D., Canagaratna, M. R.,  
Paulot, F., and Jimenez, J. L.: Characterization of a real-time tracer for isoprene  
epoxydiols-derived secondary organic aerosol (IEPOX-SOA) from aerosol mass  
spectrometer measurements, *Atmos. Chem. Phys.*, 15, 11807-11833, 2015, 10.5194/acp-  
15-11807-2015.

Hu, W. W., Palm, B., Day, D., Campuzano-Jost, P., Krechmer, J., Peng, Z., De Sá, S. S., Martin,  
S. T., Alexander, M. L., Baumann, K., Hacker, L., Kiendler-Scharr, A., Koss, A., De





- Gouw, J., Goldstein, A. H., Seco, R., Sjostedt, S., Park, J.-H., Guenther, A., Kim, S., Canonaco, F., Prevot, A., Brune, W., and Jimenez, J. L.: Long lifetime of ambient isoprene epoxydiols-derived Secondary Organic Aerosol (IEPOX-SOA) against OH oxidation and evaporation, *Atmos. Chem. Phys. Disc.*, 2016, doi: 10.5194/acp-2016-418.
- Isaacman-VanWertz, G., Yee, L. D., Kreisberg, N. M., Wernis, R., Moss, J. A., Hering, S. V., de Sá, S. S., Martin, S. T., Alexander, M. L., Palm, B. B., Hu, W., Campuzano-Jost, P., Day, D. A., Jimenez, J. L., Riva, M., Surratt, J. D., Viegas, J., Manzi, A., Edgerton, E., Baumann, K., Souza, R., Artaxo, P., and Goldstein, A. H.: Ambient Gas-Particle Partitioning of Tracers for Biogenic Oxidation, *Env. Sci. Technol.*, 2016, 10.1021/acs.est.6b01674.
- Isaacman, G., Kreisberg, N., Yee, L., Worton, D., Chan, A., Moss, J., Hering, S., and Goldstein, A.: Online derivatization for hourly measurements of gas-and particle-phase semi-volatile oxygenated organic compounds by thermal desorption aerosol gas chromatography (SV-TAG), *Atmos. Meas. Tech.*, 7, 4417-4429, 2014, 10.5194/amt-7-4417-2014.
- Jacob, D. J. and Wofsy, S. C.: Budgets of reactive nitrogen, hydrocarbons, and ozone over the Amazon forest during the wet season, *J. Geophys. Res. Atmos.*, 95, 16737-16754, 1990, 10.1029/JD095iD10p16737.
- Jacobs, M. I., Burke, W., and Elrod, M. J.: Kinetics of the reactions of isoprene-derived hydroxynitrates: gas phase epoxide formation and solution phase hydrolysis, *Atmos. Chem. Phys.*, 14, 8933-8946, 2014, 10.5194/acp-14-8933-2014.
- Jimenez, J. L., Canagaratna, M. R., Donahue, N. M., Prevot, A. S. H., Zhang, Q., Kroll, J. H., DeCarlo, P. F., Allan, J. D., Coe, H., Ng, N. L., Aiken, A. C., Docherty, K. S., Ulbrich, I. M., Grieshop, A. P., Robinson, A. L., Duplissy, J., Smith, J. D., Wilson, K. R., Lanz, V.



- A., Hueglin, C., Sun, Y. L., Tian, J., Laaksonen, A., Raatikainen, T., Rautiainen, J., Vaattovaara, P., Ehn, M., Kulmala, M., Tomlinson, J. M., Collins, D. R., Cubison, M. J., Dunlea, J., Huffman, J. A., Onasch, T. B., Alfarra, M. R., Williams, P. I., Bower, K., Kondo, Y., Schneider, J., Drewnick, F., Borrmann, S., Weimer, S., Demerjian, K., Salcedo, D., Cottrell, L., Griffin, R., Takami, A., Miyoshi, T., Hatakeyama, S., Shimono, A., Sun, J. Y., Zhang, Y. M., Dzepina, K., Kimmel, J. R., Sueper, D., Jayne, J. T., Herndon, S. C., Trimborn, A. M., Williams, L. R., Wood, E. C., Middlebrook, A. M., Kolb, C. E., Baltensperger, U., and Worsnop, D. R.: Evolution of organic aerosols in the atmosphere, *Science*, 326, 1525-1529, 2009, 10.1126/science.1180353.
- Kanakidou, M., Seinfeld, J. H., Pandis, S. N., Barnes, I., Dentener, F. J., Facchini, M. C., Van Dingenen, R., Ervens, B., Nenes, A., Nielsen, C. J., Swietlicki, E., Putaud, J. P., Balkanski, Y., Fuzzi, S., Horth, J., Moortgat, G. K., Winterhalter, R., Myhre, C. E. L., Tsigaridis, K., Vignati, E., Stephanou, E. G., and Wilson, J.: Organic aerosol and global climate modelling: a review, *Atmos. Chem. Phys.*, 5, 1053-1123, 2005, 10.5194/acp-5-1053-2005.
- Kaufman, Y. J., Tanré, D., and Boucher, O.: A satellite view of aerosols in the climate system, *Nature*, 419, 215-223, 2002.
- Kjaergaard, H. G., Knap, H. C., Ørnsø, K. B., Jørgensen, S., Crounse, J. D., Paulot, F., and Wennberg, P. O.: Atmospheric Fate of Methacrolein. 2. Formation of Lactone and Implications for Organic Aerosol Production, *J. Phys. Chem. A*, 116, 5763-5768, 2012, 10.1021/jp210853h.
- Krechmer, J. E., Coggon, M. M., Massoli, P., Nguyen, T. B., Crounse, J. D., Hu, W., Day, D. A., Tyndall, G. S., Henze, D. K., Rivera-Rios, J. C., Nowak, J. B., Kimmel, J. R., Mauldin,



- R. L., Stark, H., Jayne, J. T., Sipilä, M., Junninen, H., Clair, J. M. S., Zhang, X., Feiner, P. A., Zhang, L., Miller, D. O., Brune, W. H., Keutsch, F. N., Wennberg, P. O., Seinfeld, J. H., Worsnop, D. R., Jimenez, J. L., and Canagaratna, M. R.: Formation of low volatility organic compounds and secondary organic aerosol from isoprene hydroxyhydroperoxide low-NO oxidation, *Environ. Sci. Technol.*, 49, 10330-10339, 2015, 10.1021/acs.est.5b02031.
- Kroll, J. H., Ng, N. L., Murphy, S. M., Flagan, R. C., and Seinfeld, J. H.: Secondary organic aerosol formation from isoprene photooxidation under high-NO<sub>x</sub> conditions, *Geophys. Res. Lett.*, 32, 2005, 10.1029/2005GL023637.
- Kuhn, U., Ganzeveld, L., Thielmann, A., Dindorf, T., Schebeske, G., Welling, M., Sciare, J., Roberts, G., Meixner, F. X., Kesselmeier, J., Lelieveld, J., Kolle, O., Ciccioli, P., Lloyd, J., Trentmann, J., Artaxo, P., and Andreae, M. O.: Impact of Manaus City on the Amazon Green Ocean atmosphere: ozone production, precursor sensitivity and aerosol load, *Atmos. Chem. Phys.*, 10, 9251-9282, 2010, 10.5194/acp-10-9251-2010.
- Kuwata, M., Liu, Y., McKinney, K., and Martin, S. T.: Physical state and acidity of inorganic sulfate can regulate the production of secondary organic material from isoprene photooxidation products, *Phys. Chem. Chem. Phys.*, 17, 5670-5678, 2015, 10.1039/C4CP04942J.
- Levine, J. G., MacKenzie, A. R., Squire, O. J., Archibald, A. T., Griffiths, P. T., Abraham, N. L., Pyle, J. A., Oram, D. E., Forster, G., Brito, J. F., Lee, J. D., Hopkins, J. R., Lewis, A. C., Bauguitte, S. J. B., Demarco, C. F., Artaxo, P., Messina, P., Lathière, J., Hauglustaine, D. A., House, E., Hewitt, C. N., and Nemitz, E.: Isoprene chemistry in pristine and polluted Amazon environments: Eulerian and Lagrangian model frameworks and the strong



bearing they have on our understanding of surface ozone and predictions of rainforest exposure to this priority pollutant, *Atmos. Chem. Phys. Disc.*, 15, 24251-24310, 2015, doi: 10.5194/acpd-15-24251-2015.

Lewandowski, M., Jaoui, M., Offenberg, J., Krug, J., and Kleindienst, T.: Atmospheric oxidation of isoprene and 1, 3-butadiene: influence of aerosol acidity and relative humidity on secondary organic aerosol, *Atmos. Chem. Phys.*, 15, 3773-3783, 2015, 10.5194/acp-15-3773-2015.

Lim, H.-J., Carlton, A. G., and Turpin, B. J.: Isoprene forms secondary organic aerosol through cloud processing: Model simulations, *Environ. Sci. Technol.*, 39, 4441-4446, 2005, 10.1021/es048039h.

Lin, Y.-H., Zhang, Z., Docherty, K. S., Zhang, H., Budisulistiorini, S. H., Rubitschun, C. L., Shaw, S. L., Knipping, E. M., Edgerton, E. S., Kleindienst, T. E., Gold, A., and Surratt, J. D.: Isoprene epoxydiols as precursors to secondary organic aerosol formation: acid-catalyzed reactive uptake studies with authentic compounds, *Environ. Sci. Technol.*, 46, 250-258, 2012, 10.1021/es202554c.

Lin, Y.-H., Zhang, H., Pye, H. O. T., Zhang, Z., Marth, W. J., Park, S., Arashiro, M., Cui, T., Budisulistiorini, S. H., Sexton, K. G., Vizuete, W., Xie, Y., Luecken, D. J., Piletic, I. R., Edney, E. O., Bartolotti, L. J., Gold, A., and Surratt, J. D.: Epoxide as a precursor to secondary organic aerosol formation from isoprene photooxidation in the presence of nitrogen oxides, *Proc. Natl. Acad. Sci. USA*, 110, 6718-6723, 2013, 10.1073/pnas.1221150110.

Lin, Y.-H., Budisulistiorini, S. H., Chu, K., Siejack, R. A., Zhang, H., Riva, M., Zhang, Z., Gold, A., Kautzman, K. E., and Surratt, J. D.: Light-absorbing oligomer formation in secondary



- organic aerosol from reactive uptake of isoprene epoxydiols, *Environ. Sci. Technol.*, 48, 12012-12021, 2014, 10.1021/es503142b.
- Liu, J., D'Ambro, E. L., Lee, B. H., Lopez-Hilfiker, F. D., Zaveri, R. A., Rivera-Rios, J. C., Keutsch, F. N., Iyer, S., Kurten, T., Zhang, Z., Gold, A., Surratt, J. D., Shilling, J. E., and Thornton, J. A.: Efficient Isoprene Secondary Organic Aerosol Formation from a Non-IEPOX Pathway, *Environ. Sci. Technol.*, 2016a, 10.1021/acs.est.6b01872.
- Liu, Y., Herdinger-Blatt, I., McKinney, K., and Martin, S.: Production of methyl vinyl ketone and methacrolein via the hydroperoxyl pathway of isoprene oxidation, *Atmos. Chem. Phys.*, 13, 5715-5730, 2013, 10.5194/acp-13-5715-2013.
- Liu, Y., Kuwata, M., Strick, B. F., Geiger, F. M., Thomson, R. J., McKinney, K. A., and Martin, S. T.: Uptake of epoxydiol isomers accounts for half of the particle-phase material produced from isoprene photooxidation via the HO<sub>2</sub> pathway, *Environ. Sci. Technol.*, 49, 250-258, 2015, 10.1021/es5034298.
- Liu, Y., Brito, J., Dorris, M. R., Rivera-Rios, J. C., Seco, R., Bates, K. H., Artaxo, P., Duvoisin, S., Keutsch, F. N., Kim, S., Goldstein, A. H., Guenther, A. B., Manzi, A. O., Souza, R. A. F., Springston, S. R., Watson, T. B., McKinney, K. A., and Martin, S. T.: Isoprene photochemistry over the Amazon rain forest, *Proc. Natl. Acad. Sci. USA*, 113, 6125-6130, 2016b, 10.1073/pnas.1524136113.
- Liu, Y., Kuwata, M., McKinney, K. A., and Martin, S. T.: Uptake and release of gaseous species accompanying the reactions of isoprene photo-oxidation products with sulfate particles, *Phys. Chem. Chem. Phys.*, 18, 1595-1600, 2016c, 10.1039/C5CP04551G.
- Lopez-Hilfiker, F. D., Mohr, C., D'Ambro, E. L., Lutz, A., Riedel, T. P., Gaston, C. J., Iyer, S., Zhang, Z., Gold, A., Surratt, J. D., Lee, B. H., Kurten, T., Hu, W. W., Jimenez, J.,



- Hallquist, M., and Thornton, J. A.: Molecular composition and volatility of organic aerosol in the Southeastern US: implications for IEPOX derived SOA, *Environ. Sci. Technol.*, 2200–2209, 2016, 10.1021/acs.est.5b04769.
- Marais, E. A., Jacob, D. J., Jimenez, J. L., Campuzano-Jost, P., Day, D. A., Hu, W., Krechmer, J., Zhu, L., Kim, P. S., Miller, C. C., Fisher, J. A., Travis, K., Yu, K., Hanisco, T. F., Wolfe, G. M., Arkinson, H. L., Pye, H. O. T., Froyd, K. D., Liao, J., and McNeill, V. F.: Aqueous-phase mechanism for secondary organic aerosol formation from isoprene: application to the southeast United States and co-benefit of SO<sub>2</sub> emission controls, *Atmos. Chem. Phys.*, 16, 1603-1618, 2016, 10.5194/acp-16-1603-2016.
- Martin, S. T., Andreae, M. O., Artaxo, P., Baumgardner, D., Chen, Q., Goldstein, A. H., Guenther, A., Heald, C. L., Mayol-Bracero, O. L., McMurry, P. H., Pauliquevis, T., Pöschl, U., Prather, K. A., Roberts, G. C., Saleska, S. R., Silva Dias, M. A., Spracklen, D. V., Swietlicki, E., and Trebs, I.: Sources and properties of Amazonian aerosol particles, *Rev. Geophys.*, 48, RG2012, 2010a, 10.1029/2008RG000280.
- Martin, S. T., Andreae, M. O., Althausen, D., Artaxo, P., Baars, H., Borrmann, S., Chen, Q., Farmer, D. K., Guenther, A., Gunthe, S. S., Jimenez, J. L., Karl, T., Longo, K., Manzi, A., Müller, T., Pauliquevis, T., Petters, M. D., Prenni, A. J., Pöschl, U., Rizzo, L. V., Schneider, J., Smith, J. N., Swietlicki, E., Tota, J., Wang, J., Wiedensohler, A., and Zorn, S. R.: An overview of the Amazonian aerosol characterization experiment 2008 (AMAZE-08), *Atmos. Chem. Phys.*, 10, 11415-11438, 2010b, 10.5194/acp-10-11415-2010.
- Martin, S. T., Artaxo, P., Machado, L., Manzi, A. O., Souza, R. A. F., Schumacher, C., Wang, J., Biscaro, T., Brito, J., Calheiros, A., Jardine, K., Medeiros, A., Portela, B., Sá, S. S. d.,



- Adachi, K., Aiken, A. C., Albrecht, R., Alexander, L., Andreae, M. O., Barbosa, H. M. J., Buseck, P., Chand, D., Comstock, J. M., Day, D. A., Dubey, M., Fan, J., Fast, J., Fisch, G., Fortner, E., Giangrande, S., Gilles, M., Goldstein, A. H., Guenther, A., Hubbe, J., Jensen, M., Jimenez, J. L., Keutsch, F. N., Kim, S., Kuang, C., Laskin, A., McKinney, K., Mei, F., Miller, M., Nascimento, R., Pauliquevis, T., Pekour, M., Peres, J., Petäjä, T., Pöhlker, C., Pöschl, U., Rizzo, L., Schmid, B., Shilling, J. E., Dias, M. A. S., Smith, J. N., Tomlinson, J. M., Tóta, J., and Wendisch, M.: The Green ocean Amazon Experiment (GoAmazon2014/5) observes pollution affecting gases, aerosols, clouds, and rainfall over the rain forest, *B. Am. Meteorol. Soc.*, 2016a, doi:10.1175/BAMS-D-15-00221.1.
- Martin, S. T., Artaxo, P. E., Chen, Q., Guenther, A. B., Gunthe, S. S., Jimenez, J. L., Manzi, A., Prenni, K. L., Poschl, U., Schneider, J., and Swietlicki, E.: AMAZE-08 Aerosol Characterization and Meteorological Data, Central Amazon Basin: 2008. ORNL Distributed Active Archive Center, 2016b.
- Martin, S. T., Artaxo, P., Machado, L. A. T., Manzi, A. O., Souza, R. A. F., Schumacher, C., Wang, J., Andreae, M. O., Barbosa, H. M. J., Fan, J., Fisch, G., Goldstein, A. H., Guenther, A., Jimenez, J. L., Pöschl, U., Silva Dias, M. A., Smith, J. N., and Wendisch, M.: Introduction: observations and modeling of the green ocean Amazon (GoAmazon2014/5), *Atmos. Chem. Phys.*, 16, 4785-4797, 2016c, 10.5194/acp-16-4785-2016.
- Mather, J. H. and Voyles, J. W.: The ARM Climate Research Facility: A review of structure and capabilities, *B. Am. Meteorol. Soc.*, 94, 377-392, 2013, <http://dx.doi.org/ezp-prod1.hul.harvard.edu/10.1175/BAMS-D-11-00218.1>.



- McNeill, V. F., Woo, J. L., Kim, D. D., Schwier, A. N., Wannell, N. J., Sumner, A. J., and Barakat, J. M.: Aqueous-phase secondary organic aerosol and organosulfate formation in atmospheric aerosols: a modeling study, *Environ. Sci. Technol.*, 46, 8075-8081, 2012, 10.1021/es3002986.
- Medeiros, A., Souza, R. A. F., and Martin, S. T., in preparation.
- Nel, A.: Air pollution-related illness: effects of particles, *Science*, 308, 804-806, 2005.
- Nguyen, T. B., Coggon, M. M., Bates, K. H., Zhang, X., Schwantes, R. H., Schilling, K. A., Loza, C. L., Flagan, R. C., Wennberg, P. O., and Seinfeld, J. H.: Organic aerosol formation from the reactive uptake of isoprene epoxydiols (IEPOX) onto non-acidified inorganic seeds, *Atmos. Chem. Phys.*, 14, 3497-3510, 2014, 10.5194/acp-14-3497-2014.
- Nguyen, T. B., Bates, K. H., Crouse, J. D., Schwantes, R. H., Zhang, X., Kjaergaard, H. G., Surratt, J. D., Lin, P., Laskin, A., Seinfeld, J. H., and Wennberg, P. O.: Mechanism of the hydroxyl radical oxidation of methacryloyl peroxyxynitrate (MPAN) and its pathway toward secondary organic aerosol formation in the atmosphere, *Phys. Chem. Chem. Phys.*, 17, 17914-17926, 2015, 10.1039/C5CP02001H.
- Pandis, S. N., Paulson, S. E., Seinfeld, J. H., and Flagan, R. C.: Aerosol formation in the photooxidation of isoprene and  $\beta$ -pinene, *Atmos. Environ., Part A*, 25, 997-1008, 1991, 10.1016/0960-1686(91)90141-S.
- Paulot, F., Crouse, J. D., Kjaergaard, H. G., Kürten, A., Clair, J. M. S., Seinfeld, J. H., and Wennberg, P. O.: Unexpected epoxide formation in the gas-phase photooxidation of isoprene, *Science*, 325, 730-733, 2009, 10.1126/science.1172910.
- Pope III, C. A. and Dockery, D. W.: Health effects of fine particulate air pollution: lines that connect, *J Air Waste Manag Assoc*, 56, 709-742, 2006.





- Pöschl, U., Martin, S. T., Sinha, B., Chen, Q., Gunthe, S. S., Huffman, J. A., Borrmann, S., Farmer, D. K., Garland, R. M., Helas, G., Jimenez, J. L., King, S. M., Manzi, A., Mikhailov, E., Pauliquevis, T., Petters, M. D., Prenni, A. J., Roldin, P., Rose, D., Schneider, J., Su, H., Zorn, S. R., Artaxo, P., and Andreae, M. O.: Rainforest aerosols as biogenic nuclei of clouds and precipitation in the Amazon, *Science*, 329, 1513-1516, 2010, 10.1126/science.1191056.
- Ramanathan, V., Crutzen, P., Kiehl, J., and Rosenfeld, D.: Aerosols, climate, and the hydrological cycle, *Science*, 294, 2119-2124, 2001.
- Riedel, T., Lin, Y.-H., Zhang, Z., Chu, K., Thornton, J., Vizuete, W., Gold, A., and Surratt, J.: Constraining condensed-phase formation kinetics of secondary organic aerosol components from isoprene epoxydiols, *Atmos. Chem. Phys.*, 16, 1245-1254, 2016, DOI: 10.5194/acp-16-1245-2016.
- Riva, M., Bell, D. M., Hansen, A.-M. K., Drozd, G. T., Zhang, Z., Gold, A., Imre, D., Surratt, J. D., Glasius, M., and Zelenyuk, A.: Effect of organic coatings, humidity and aerosol acidity on multiphase chemistry of isoprene epoxydiols, *Environ. Sci. Technol.*, 50, 5580-5588, 2016a, 10.1021/acs.est.5b06050.
- Riva, M., Budisulistiorini, S. H., Chen, Y., Zhang, Z., D'Ambro, E. L., Zhang, X., Gold, A., Turpin, B. J., Thornton, J. A., Canagaratna, M. R., and Surratt, J. D.: Chemical characterization of secondary organic aerosol from oxidation of isoprene hydroxyhydroperoxides, *Environ. Sci. Technol.*, 2016b, 10.1021/acs.est.6b02511.
- Robinson, N. H., Hamilton, J. F., Allan, J. D., Langford, B., Oram, D. E., Chen, Q., Docherty, K., Farmer, D. K., Jimenez, J. L., Ward, M. W., Hewitt, C. N., Barley, M. H., Jenkin, M. E., Rickard, A. R., Martin, S. T., McFiggans, G., and Coe, H.: Evidence for a significant



- proportion of Secondary Organic Aerosol from isoprene above a maritime tropical forest, *Atmos. Chem. Phys.*, 11, 1039-1050, 2011, 10.5194/acp-11-1039-2011.
- Rohrer, F., Lu, K., Hofzumahaus, A., Bohn, B., Brauers, T., Chang, C.-C., Fuchs, H., Haseler, R., Holland, F., Hu, M., Kita, K., Kondo, Y., Li, X., Lou, S., Oebel, A., Shao, M., Zeng, L., Zhu, T., Zhang, Y., and Wahner, A.: Maximum efficiency in the hydroxyl-radical-based self-cleansing of the troposphere, *Nat. Geosci.*, 7, 559-563, 2014, 10.1038/ngeo2199.
- Romer, P. S., Duffey, K. C., Wooldridge, P. J., Allen, H. M., Ayres, B. R., Brown, S. S., Brune, W. H., Crouse, J. D., de Gouw, J., Draper, D. C., Feiner, P. A., Fry, J. L., Goldstein, A. H., Koss, A., Misztal, P. K., Nguyen, T. B., Olson, K., Teng, A. P., Wennberg, P. O., Wild, R. J., Zhang, L., and Cohen, R. C.: The lifetime of nitrogen oxides in an isoprene-dominated forest, *Atmos. Chem. Phys.*, 16, 7623-7637, 2016, 10.5194/acp-16-7623-2016.
- Rummel, U., Ammann, C., Kirkman, G., Moura, M., Foken, T., Andreae, M., and Meixner, F.: Seasonal variation of ozone deposition to a tropical rain forest in southwest Amazonia, *Atmos. Chem. Phys.*, 7, 5415-5435, 2007, 10.5194/acp-7-5415-2007.
- Schmid, B., Tomlinson, J. M., Hubbe, J. M., Comstock, J. M., Mei, F., Chand, D., Pekour, M. S., Kluzek, C. D., Andrews, E., Biraud, S. C., and McFarquhar, G. M.: The DOE ARM aerial facility, *B. Am. Meteorol. Soc.*, 95, 723-742, 2014, 10.1175/BAMS-D-13-00040.1.
- Slowik, J. G., Brook, J., Chang, R. Y. W., Evans, G. J., Hayden, K., Jeong, C. H., Li, S. M., Liggio, J., Liu, P. S. K., McGuire, M., Mihele, C., Sjostedt, S., Vlasenko, A., and Abbatt, J. P. D.: Photochemical processing of organic aerosol at nearby continental sites: contrast between urban plumes and regional aerosol, *Atmos. Chem. Phys.*, 11, 2991-3006, 2011, 10.5194/acp-11-2991-2011.



- St. Clair, J. M., Rivera-Rios, J. C., Crouse, J. D., Knap, H. C., Bates, K. H., Teng, A. P., Jørgensen, S., Kjaergaard, H. G., Keutsch, F. N., and Wennberg, P. O.: Kinetics and products of the reaction of the first-generation isoprene hydroxy hydroperoxide (ISOPOOH) with OH, *J. Phys. Chem. A*, 2015, 10.1021/acs.jpca.5b06532.
- Surratt, J. D., Murphy, S. M., Kroll, J. H., Ng, N. L., Hildebrandt, L., Sorooshian, A., Szmigielski, R., Vermeylen, R., Maenhaut, W., Claeys, M., Flagan, R. C., and Seinfeld, J. H.: Chemical composition of secondary organic aerosol formed from the photooxidation of isoprene, *J. Phys. Chem. A*, 110, 9665-9690, 2006, 10.1021/jp061734m.
- Surratt, J. D., Lewandowski, M., Offenberg, J. H., Jaoui, M., Kleindienst, T. E., Edney, E. O., and Seinfeld, J. H.: Effect of acidity on secondary organic aerosol formation from isoprene, *Environ. Sci. Technol.*, 41, 5363-5369, 2007a, 10.1021/es0704176.
- Surratt, J. D., Kroll, J. H., Kleindienst, T. E., Edney, E. O., Claeys, M., Sorooshian, A., Ng, N. L., Offenberg, J. H., Lewandowski, M., Jaoui, M., Flagan, R. C., and Seinfeld, J. H.: Evidence for organosulfates in secondary organic aerosol, *Environ. Sci. Technol.*, 41, 517-527, 2007b, 10.1021/es062081q.
- Surratt, J. D., Chan, A. W., Eddingsaas, N. C., Chan, M., Loza, C. L., Kwan, A. J., Hersey, S. P., Flagan, R. C., Wennberg, P. O., and Seinfeld, J. H.: Reactive intermediates revealed in secondary organic aerosol formation from isoprene, *Proc. Natl. Acad. Sci. USA*, 107, 6640-6645, 2010, 10.1073/pnas.0911114107.
- Torres, A. and Buchan, H.: Tropospheric nitric oxide measurements over the Amazon Basin, *J. Geophys. Res. Atmos.*, 93, 1396-1406, 1988, 10.1029/JD093iD02p01396.



- Trebs, I., Mayol-Bracero, O. L., Pauliquevis, T., Kuhn, U., Sander, R., Ganzeveld, L., Meixner, F. X., Kesselmeier, J., Artaxo, P., and Andreae, M. O.: Impact of the Manaus urban plume on trace gas mixing ratios near the surface in the Amazon Basin: Implications for the NO-NO<sub>2</sub>-O<sub>3</sub> photostationary state and peroxy radical levels, *J. Geophys. Res. Atmos.*, 117, D05307, 2012, doi:10.1029/2011JD016386.
- Ulbrich, I., Canagaratna, M., Zhang, Q., Worsnop, D., and Jimenez, J.: Interpretation of organic components from Positive Matrix Factorization of aerosol mass spectrometric data, *Atmos. Chem. Phys.*, 9, 2891-2918, 2009, 10.5194/acp-9-2891-2009.
- Valin, L., Russell, A., and Cohen, R.: Variations of OH radical in an urban plume inferred from NO<sub>2</sub> column measurements, *Geophys. Res. Lett.*, 40, 1856-1860, 2013, 10.1002/grl.50267.
- Volkamer, R., San Martini, F., Molina, L. T., Salcedo, D., Jimenez, J. L., and Molina, M. J.: A missing sink for gas-phase glyoxal in Mexico City: Formation of secondary organic aerosol, *Geophys. Res. Lett.*, 34, L19807, 2007, 10.1029/2007GL030752.
- Wang, W., Kourtchev, I., Graham, B., Cafmeyer, J., Maenhaut, W., and Claeys, M.: Characterization of oxygenated derivatives of isoprene related to 2-methyltetrols in Amazonian aerosols using trimethylsilylation and gas chromatography/ion trap mass spectrometry, *Rap. Commun. Mass Spectrom.*, 19, 1343-1351, 2005, 10.1002/rcm.1940.
- Wennberg, P.: Let's abandon the "high NO<sub>x</sub>" and "low NO<sub>x</sub>" terminology, *IGAC news*, 50, 3-4, 2013.
- Worton, D. R., Surratt, J. D., LaFranchi, B. W., Chan, A. W. H., Zhao, Y., Weber, R. J., Park, J.-H., Gilman, J. B., de Gouw, J., Park, C., Schade, G., Beaver, M., Clair, J. M. S., Crouse, J., Wennberg, P., Wolfe, G. M., Harrold, S., Thornton, J. A., Farmer, D. K., Docherty, K.



- S., Cubison, M. J., Jimenez, J.-L., Frossard, A. A., Russell, L. M., Kristensen, K., Glasius, M., Mao, J., Ren, X., Brune, W., Browne, E. C., Pusede, S. E., Cohen, R. C., Seinfeld, J. H., and Goldstein, A. H.: Observational insights into aerosol formation from isoprene, *Environ. Sci. Technol.*, 47, 11403-11413, 2013, 10.1021/es4011064.
- Xu, L., Guo, H., Boyd, C. M., Klein, M., Bougiatioti, A., Cerully, K. M., Hite, J. R., Isaacman-VanWertz, G., Kreisberg, N. M., Knote, C., Olson, K., Koss, A., Goldstein, A. H., Hering, S. V., de Gouw, J., Baumann, K., Lee, S.-H., Nenes, A., Weber, R. J., and Ng, N. L.: Effects of anthropogenic emissions on aerosol formation from isoprene and monoterpenes in the southeastern United States, *Proc. Natl. Acad. Sci. USA*, 112, 37-42, 2015, 10.1073/pnas.1417609112.
- Zhang, Q., Jimenez, J. L., Canagaratna, M. R., Allan, J. D., Coe, H., Ulbrich, I., Alfarra, M. R., Takami, A., Middlebrook, A. M., Sun, Y. L., Dzepina, K., Dunlea, E., Docherty, K., DeCarlo, P. F., Salcedo, D., Onasch, T., Jayne, J. T., Miyoshi, T., Shimono, A., Hatakeyama, S., Takegawa, N., Kondo, Y., Schneider, J., Drewnick, F., Borrmann, S., Weimer, S., Demerjian, K., Williams, P., Bower, K., Bahreini, R., Cottrell, L., Griffin, R. J., Rautiainen, J., Sun, J. Y., Zhang, Y. M., and Worsnop, D. R.: Ubiquity and dominance of oxygenated species in organic aerosols in anthropogenically-influenced Northern Hemisphere midlatitudes, *Geophys. Res. Lett.*, 34, L13801, 2007, 10.1029/2007GL029979.



### List of Tables

Group	NO <sub>y</sub> range (ppb)	Fit slope	Fit intercept	Fit $R^2$
1	< 0.66	2.16	-0.13	0.75
2	0.66 – 0.92	1.48	-0.04	0.64
3	0.92 – 1.55	0.78	0.06	0.24
4	1.55 – 2.45	0.71	-0.01	0.44
5	> 2.45	0.55	-0.02	0.62

**Table 1.** Parameters associated with NO<sub>y</sub> groupings in Figure 6. Listed are the NO<sub>y</sub> concentrations and the parameters for least-squares linear fits to each group.  $R^2$  represents the coefficient of determination.



Symbol	Description	Unit
$M$	mass concentration of IEPOX-derived PM	$\mu\text{g m}^{-3}$
$t$	time	h
$k_p$	zero-order rate coefficient for production under background conditions	$\mu\text{g m}^{-3} \text{h}^{-1}$
$k_L$	first-order rate coefficient for loss under background conditions	$\text{h}^{-1}$
$\alpha$	multiplicative factor representing the effects of Manaus pollution on rate coefficients	
$\tau$	characteristic time of a process (e.g., production, loss, or transport)	h
Subscript $tr$	Refers to transport	
Subscript $bg$	Refers to background conditions	
Subscript $pol$	Refers to polluted conditions	
Subscript 0	Refers to an initial state (i.e., just upwind of Manaus)	
Subscript $P$	Refers to production processes	
Subscript $L$	Refers to loss processes	

**Table 2.** Descriptions and units of symbols in the model.



	Loading ( $\mu\text{g m}^{-3}$ ) for background conditions		Loading ( $\mu\text{g m}^{-3}$ ) for polluted conditions		Ratio $\zeta$	
	Low sulfate	High sulfate	Low sulfate	High sulfate	Low sulfate	High sulfate
	IEPOX- SOA factor	[0.037, 0.093]	[0.57, 0.95]	[0.022, 0.039]	[0.21, 0.35]	0.47

**Table 3.** Interquartile intervals of IEPOX-SOA factor loadings observed for background and polluted conditions. Background and polluted conditions correspond to approximately 0.5 ppb and 2 ppb of  $\text{NO}_y$ , respectively. The table also lists the resulting ratio  $\zeta$  of the median factor loading under polluted compared to background conditions.





Model case	Parameter values				Initial condition
	$k_P$	$k_L$	$\alpha_P$	$\alpha_L$	$M_0$
1. Vary $k_P$	0 to 0.2	0.018	0.1	3	0.23
2. Vary $k_L$	0.065	0.001 to 1	0.1	3	0.23

**Table 4.** Parameter values and initial conditions used in model cases. Descriptions and units are listed in Table 2. The  $M_0$  value is based on the mean IEPOX-SOA factor loading that was measured from 14:00-16:00 UTC (10:00-12:00 local time) at a regional background site during two months of the wet season in 2008 (Chen et al., 2015). For comparison, a similar value of  $0.19 \mu\text{g m}^{-3}$  was obtained during the present study as the mean value observed at the T3 site for  $\text{NO}_y < 1$  ppb (14:00-16:00 UTC).



## List of Figures

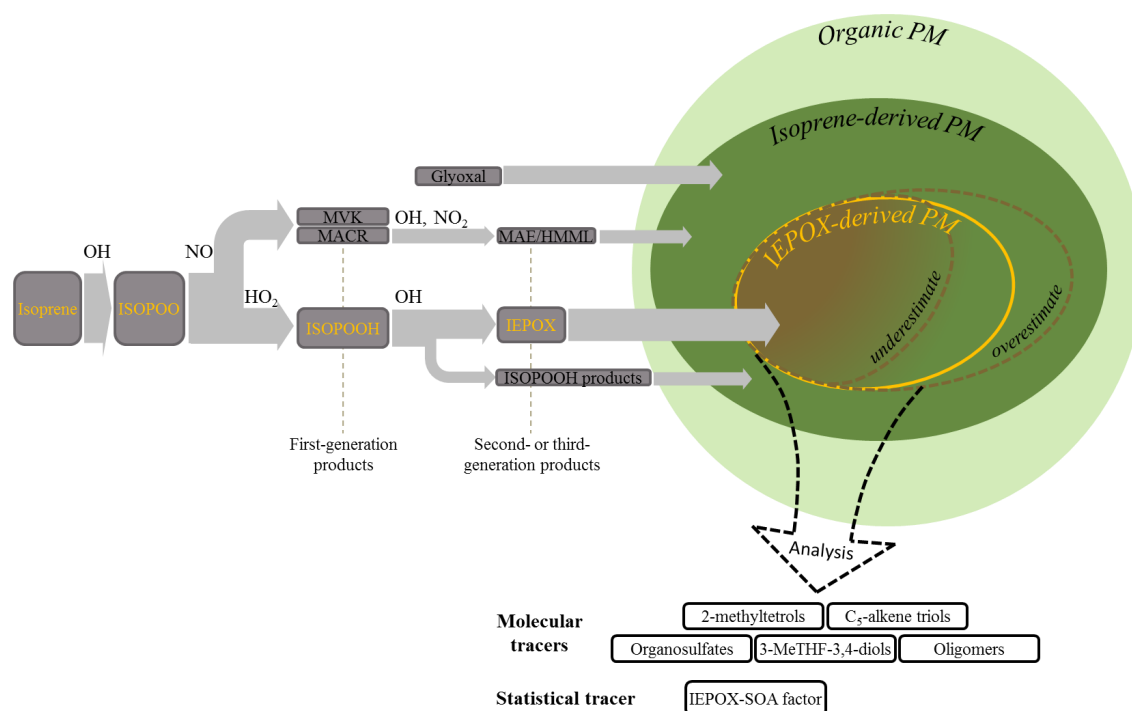


**Figure 1.** Schematic diagram for the production of IEPOX-derived PM from the photooxidation of isoprene. Organic peroxy radicals (ISOPOO), produced by OH attack and O<sub>2</sub> addition to isoprene, are scavenged along NO or HO<sub>2</sub> pathways. By the HO<sub>2</sub> pathway, organic hydroperoxides (ISOPOOH) are first-generation products that react with additional OH to produce isoprene epoxydiols (IEPOX). The IEPOX species undergo reactive uptake into particles, ultimately producing IEPOX-derived particulate matter. Arrow thickness qualitatively illustrates the relative importance (i.e., mass flux) of a reaction channel under background conditions. Gray and green background colors indicate species in the gas and particle phases, respectively. The light-green disk represents the total organic PM. Within that disk, the contribution by isoprene-derived PM, including compounds produced both IEPOX and non-IEPOX pathways, is represented by the dark-green oval. Inside that oval, the contribution by IEPOX-derived PM is represented by the yellow oval region. The color gradient between brown and dark green illustrates the chemical modification of the IEPOX-derived PM over time. The large dashed black arrow represents the analytical methods that use different types of molecular and statistical tracers (listed in the boxes) to quantify the IEPOX-derived PM mass concentrations. For simplicity, the figure omits the many routes leading to the production of glyoxal (Fu et al., 2008), possible ISOPOO isomerization when NO and HO<sub>2</sub> concentrations are sufficiently low (Crouse et al., 2011; Liu et al., 2016a), second-generation production of peroxyacetic nitric anhydride (Lin et al., 2013; Nguyen et al., 2015), and particle water and other inorganic components. 3-methyltetrahydrofuran-3,4-diols are abbreviated as 3-MeTHF-3,4-diols. Other abbreviations are provided in the main text.

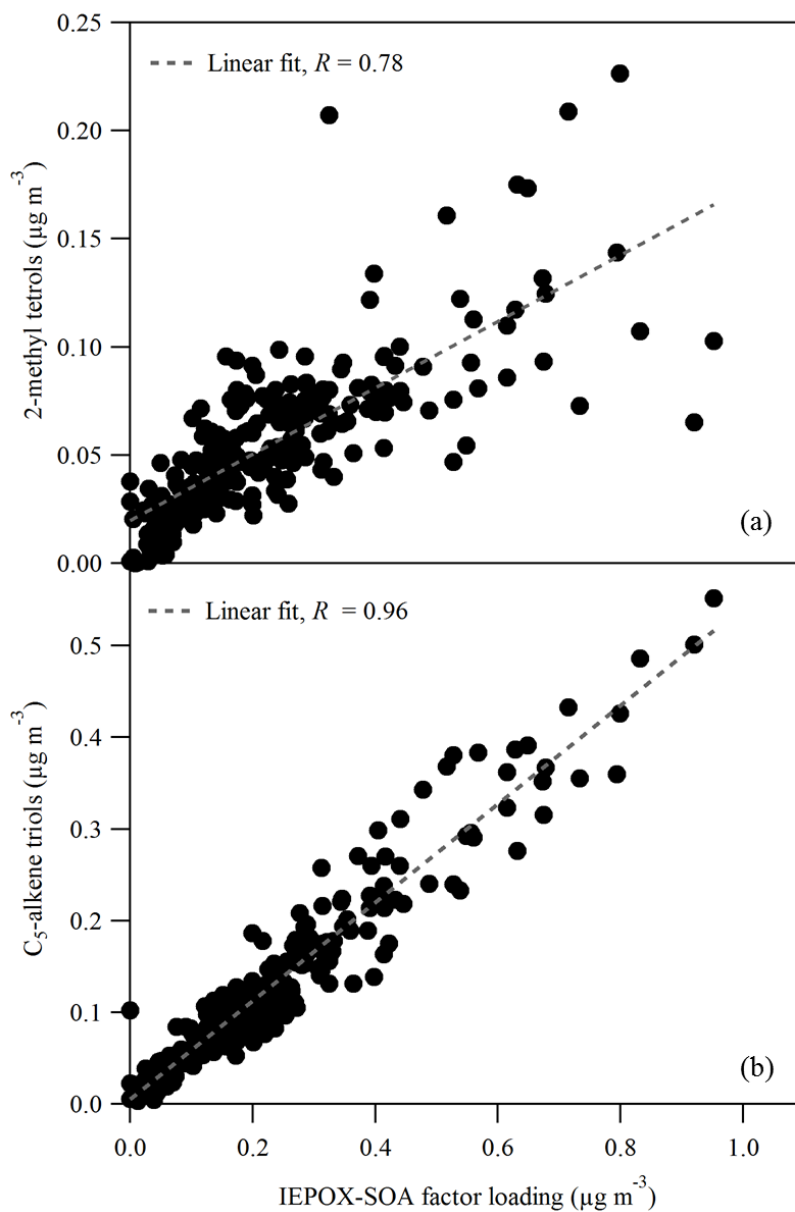


**Figure 2.** Scatter plot of the loading of the IEPOX-SOA factor derived from analysis of the AMS data set and the mass concentrations of C<sub>5</sub>-alkene triols and 2-methyltetrols measured by SV-TAG. All data collected during IOP1 are included, meaning that the plotted data are not limited to afternoon time periods.

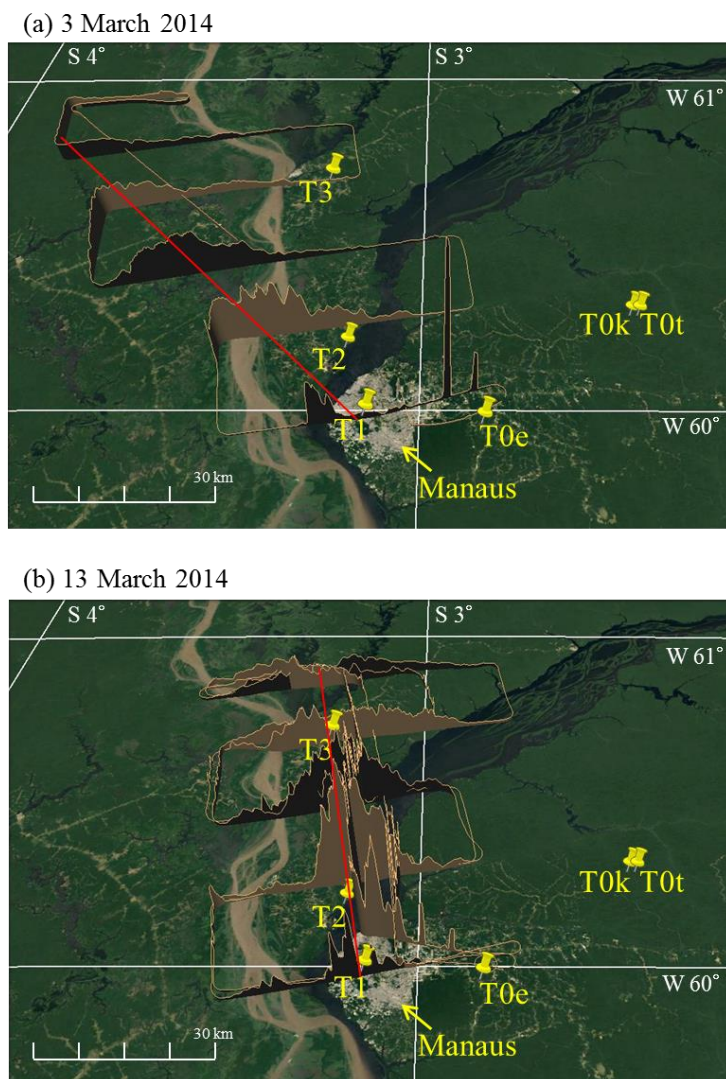


**Figure 3.** Visualization of the Manaus pollution plume by plotting particle number concentrations in the vertical axis. Observations took place on flights from late morning to early afternoon on (a) March 3, 2014, 17:45 – 19:26 UTC, and (b) March 13, 2014, 14:14 – 17:21 UTC. Local time is UTC minus 4 h. The red lines guide the eye through the central axis of the plume. The direction and extent of the plume was observed by the G-1 aircraft within the atmospheric boundary layer downwind of Manaus. Measured particle number concentrations are plotted on a vertical axis on top of an image of land cover in the horizontal plane. Particle concentrations in the center of the plume ranged from 10,000 to 25,000  $\text{cm}^{-3}$  nearby Manaus. Yellow pins indicate the locations of some of the GoAmazon2014/5 research sites, including T3 (Martin et al., 2016c).

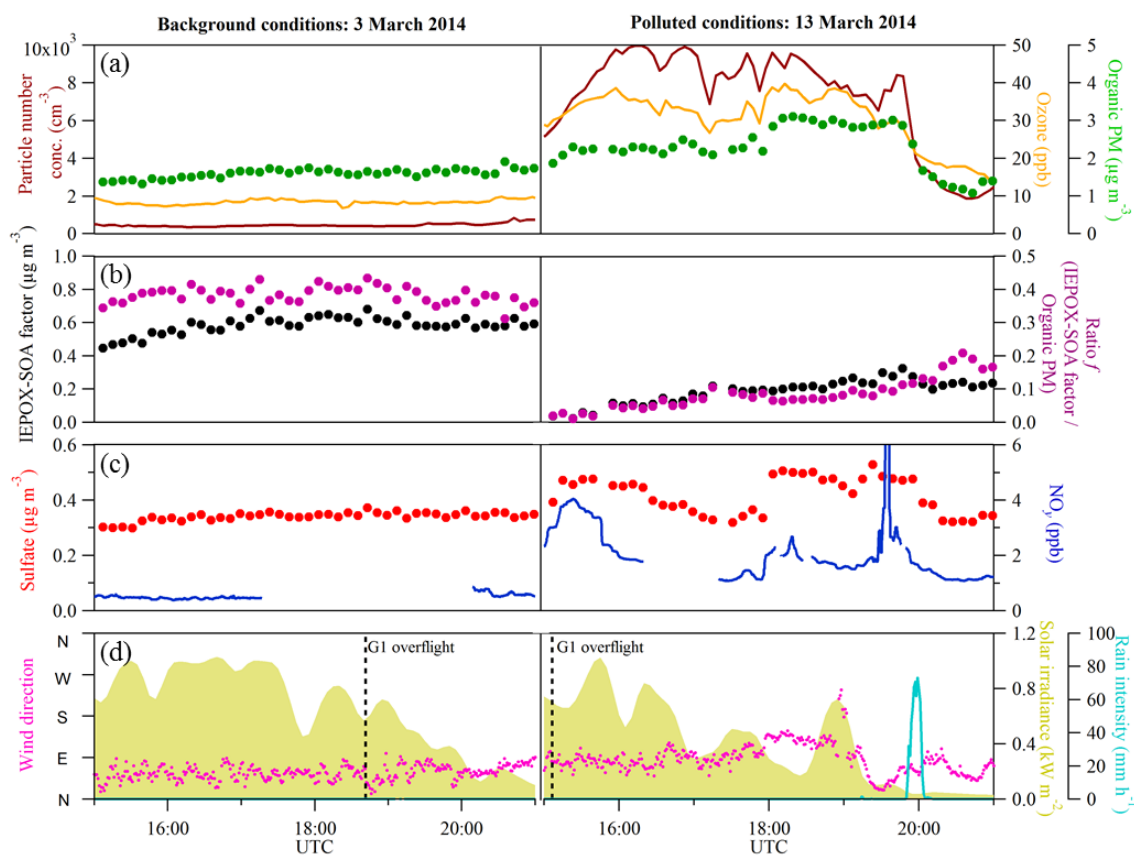


**Figure 4.** Case studies of (left) background and (right) polluted air masses passing over T3 on afternoons of March 3 and 13, 2014. (a) Ozone, particle number, and organic mass concentration. (b) IEPOX-SOA factor loading and the ratio  $f$  of the factor loading to the organic PM concentration. (c) Sulfate and  $\text{NO}_y$  concentrations. (d) Wind direction, rain intensity, and solar irradiance. Local time is UTC minus 4 h. Time points of overflights at 500 m by the G-1 research aircraft are marked by the dashed line (Martin et al., 2016a).

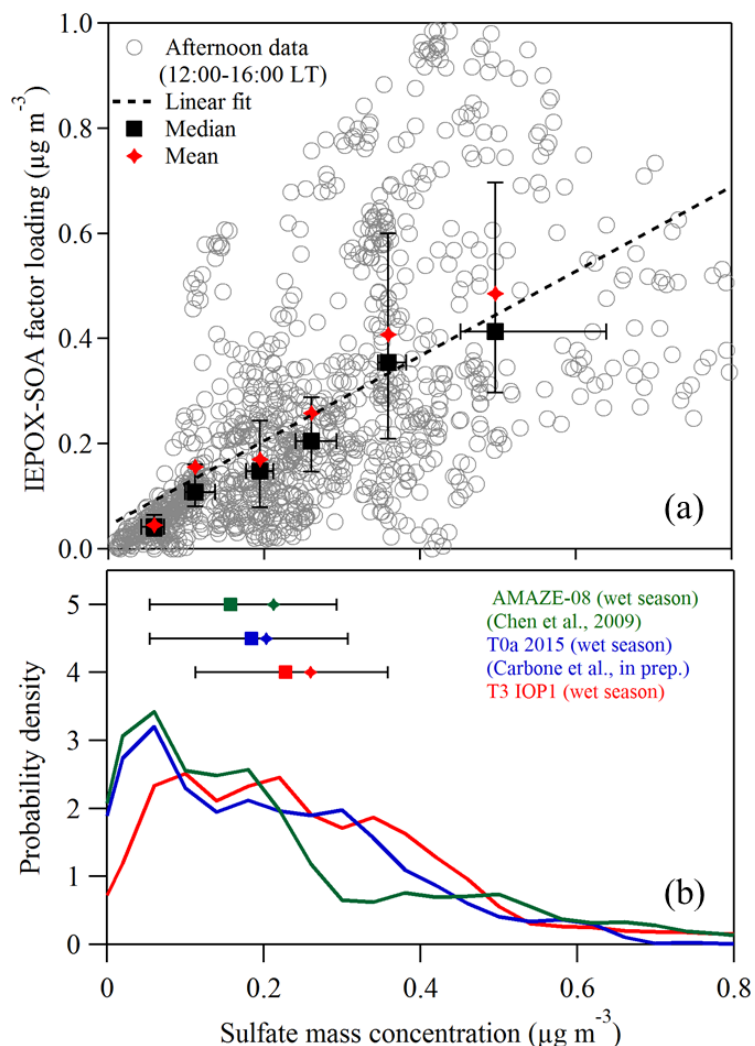


**Figure 5.** (a) Scatter plot of sulfate mass concentration and IEPOX-SOA factor loading. A least-squares linear fit is represented by the dashed line ( $R^2 = 0.37$ ). The data set was collected into six subsets based on sulfate concentration to calculate statistics. Medians (squares) and means (diamonds) of each subset are plotted. Whiskers on the medians represent the interquartile ranges. (b) Probability density function of sulfate mass concentration at the background site T0t (“TT34”) north of Manaus in the wet season of 2008 (Chen et al., 2009; Martin et al., 2010b; Martin et al., 2016b), at the background site T0a (“ATTO”) northeast of Manaus in the wet season of 2015 (Andreae et al., 2015), and at T3 during the wet season of 2014 (IOP1). The plotted data sets were recorded during local afternoons (12:00-16:00 local time; 16:00-20:00 UTC). Means (diamonds), medians (squares), and interquartile range (whiskers) are shown for the probability density functions.

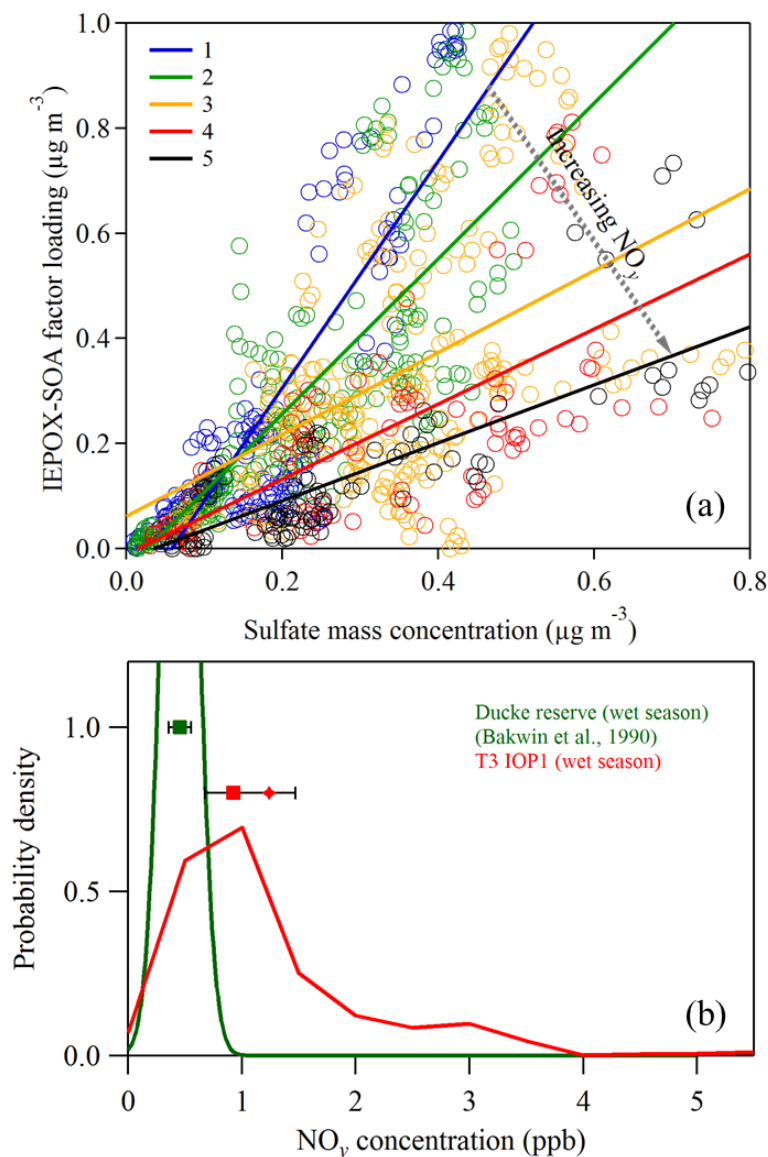


**Figure 6.** (a) Scatter plot of sulfate mass concentration and IEPOX-SOA factor loading for local afternoon (12:00-16:00 local time; 16:00-20:00 UTC). The data sets were collected into five subsets, colored and labeled 1 to 5, based on  $\text{NO}_y$  concentration. Table 1 presents the parameters of the five least-squares linear fits represented by the colored lines in the figure. (b) Probability density function of  $\text{NO}_y$  concentration at a background site nearby Manaus in the wet season of 1987 (Bakwin et al., 1990) and at T3 during the wet season of 2014 (IOPI) (afternoon data). Means (diamonds), medians (squares), and interquartile range (whiskers) are shown for the probability density functions. Additional analysis of panel (a) is discussed in the Supplement (Section S5) related to Figure S5.



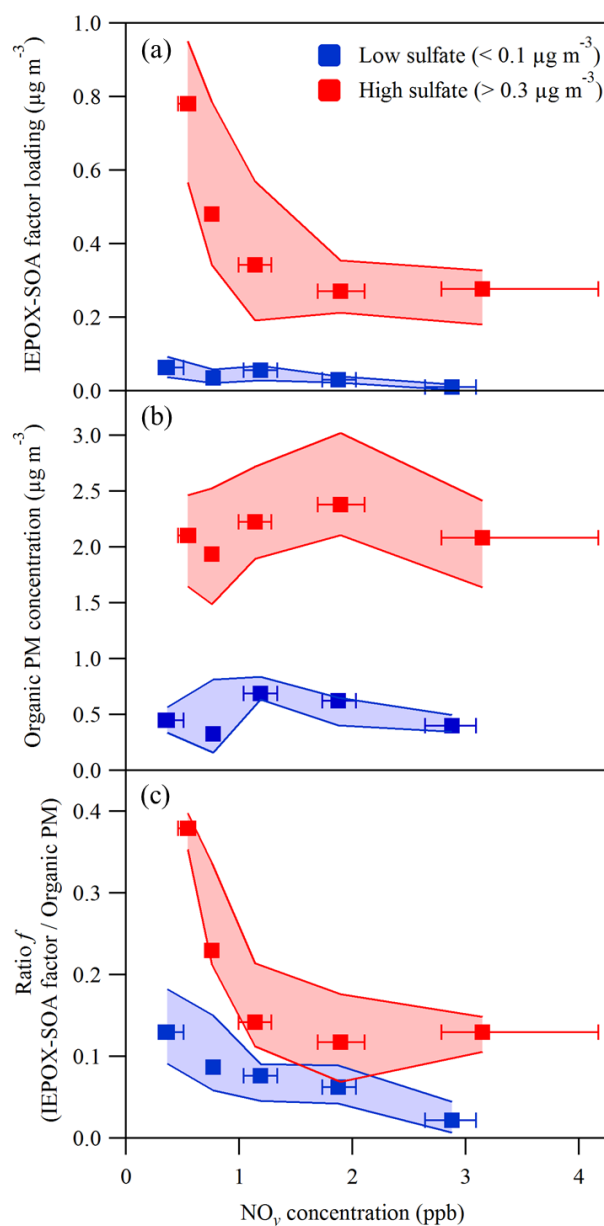


**Figure 7.** Dependence on  $\text{NO}_y$  concentration of (a) IEPOX-SOA factor loading, (b) organic mass concentration, and (c) the ratio  $f$  of the IEPOX-SOA factor loading to the organic PM concentration. Data are segregated by low ( $< 0.1 \mu\text{g m}^{-3}$ ) and high ( $> 0.3 \mu\text{g m}^{-3}$ ) sulfate mass concentration and grouped into five levels of  $\text{NO}_y$  concentration (Figure 6). Squares represent medians of each group. Interquartile ranges are represented by whiskers along the abscissa and shading along the ordinate. The plotted data sets were recorded during local afternoon (12:00-16:00 local time; 16:00-20:00 UTC).



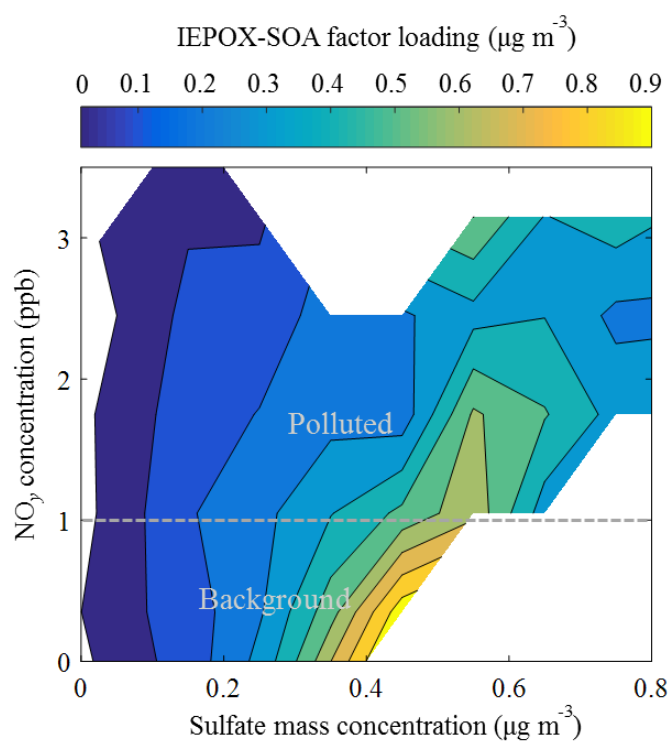


**Figure 8.** Contours of IEPOX-SOA factor loading for sulfate and NO<sub>y</sub> concentrations. The plotted data were recorded during local afternoon (12:00-16:00 local time; 16:00-20:00 UTC). Typical transition between regimes of background and polluted conditions for the region downwind of Manaus are approximately represented by the dashed gray line.

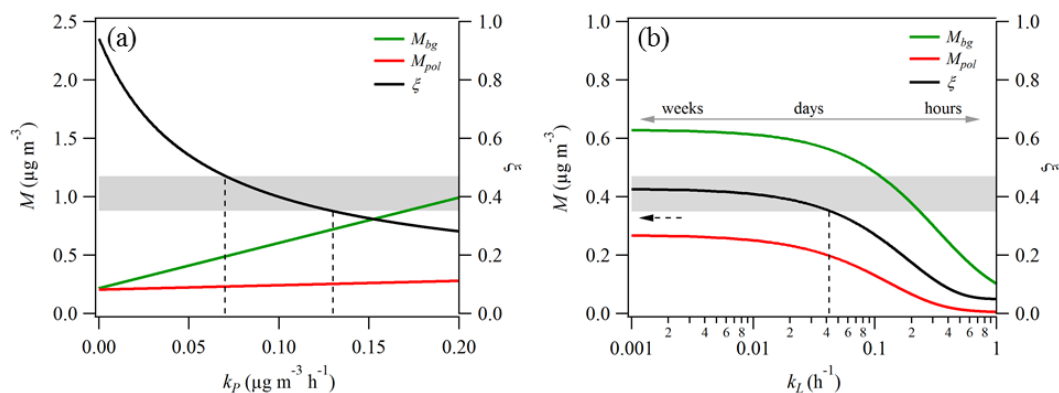


**Figure 9.** Modeled IEPOX-derived PM mass concentrations  $M_{pol}$  and  $M_{bg}$  at the T3 site under polluted compared to background conditions. The ratio  $\zeta$  of concentrations (i.e.,  $M_{pol}/M_{bg}$ ) is also plotted. Panels a and b correspond to the two model Cases 1 and 2 listed in Table 4 and described in the text. Gray shading indicates the range of observed values of  $\zeta$  across low and high sulfate concentrations. Dashed lines indicate the intersection of modeled and observed values of  $\zeta$  and the corresponding constrained values of  $k_p$  or  $k_L$  along the abscissa. Labels above the double-headed arrow in panel b correspond to characteristic times (i.e.,  $k_L^{-1}$ ). The dashed black arrow in panel b communicates that the observed values of  $\zeta$  provide no constraint on the lower limit of  $k_L$ .